Bioactive exometabolites drive maintenance competition in simple bacterial communities

John L. Chodkowski[1] and Ashley Shade[1,2,3*]

[1]Department of Microbiology and Molecular Genetics, Michigan State University, East Lansing, MI 48824, USA

[2]Department of Plant, Soil and Microbial Sciences, Michigan State University, East Lansing, MI 48824, USA

[3]Program in Ecology, Evolutionary Biology and Behavior, Michigan State University, 10 East Lansing, MI 48824, USA

* Corresponding author and material requests. Email: shadeash@msu.edu; ORCiD: 0000-0002-7189-3067

Abstract

During prolonged resource limitation, bacterial cells can persist in metabolically active states of non-growth. These maintenance periods, such as those experienced by cells in stationary phase cultures, can, perhaps counterintuitively, include upregulation of cellular secondary metabolism and release of exometabolites into the local environment, at the cost of an energetic commitment to growth. As resource limitation is a characteristic feature of many habitats that harbor environmental microbial communities, we hypothesized that neighboring bacterial populations employ exometabolites to compete or cooperate during maintenance, and that these

exometabolite-facilitated interactions can drive community outcomes. Here, we evaluated the consequences of exometabolite interactions over stationary phase among three well-known environmental bacterial strains: *Burkholderia thailandensis* E264 (ATCC 700388), *Chromobacterium violaceum* ATCC 31532, and *Pseudomonas syringae* pv.*tomato* DC3000 (ATCC BAA-871). We assembled these stains into laboratory-scale synthetic communities that only permitted chemical interactions among them. We compared the responses (transcripts) and behaviors (exometabolites) of each member with and without neighbors. We found that transcriptional dynamics were altered in the presence of different neighbors, and that these changes could be attributed to the production of or response to bioactive exometabolites employed for competition during maintenance. *B. thailandensis* was especially influential and competitive within its communities, as it consistently upregulated additional biosynthetic gene clusters involved in the production of bioactive exometabolites for both exploitative and interference competition. Additionally, some of these bioactive exometabolites were upregulated and produced in a non-additive manner in the 3-member community. These results demonstrate that the active investment in competition during maintenance can contribute to both bacterial population fitness and community-level outcomes. It also suggests that the traditional concept of defining competitiveness by growth outcomes may be too narrow, and that maintenance competition could be an alternative measure.

Introduction

Bacteria interact with other bacteria and their environment within complex, multi-species communities. Bacterial interactions rely on the ability to sense and respond to both biotic and abiotic stimuli (Stock et al., 2000; Browning and Busby, 2004). These stimuli include physical, chemical or molecular cues, and can alter bacterial behaviors (Pietschke et al., 2017; Garren et al., 2016), and ultimately, can also alter community functioning (Kato et al., 2005; Steinweg et al., 2013). It is expected that interspecies interactions play an important role in shaping microbial community dynamics (Aziz et al., 2015). However, multiple stimuli in the environment make it difficult to disentangle the separate influences of abiotic versus biotic stimuli on microbial community dynamics (Orr et al., 2020). Therefore, efforts to characterize and distinguish community responses to biotic stimuli, such as those that facilitate interspecies interactions, will provide insights into the specific roles that microbial interactions play in shaping their communities (Little et al., 2008).

Interspecies interactions can be facilitated through small molecules (Phelan et al., 2011). Extracellular small molecules are collectively referred to as exometabolites (Kell et al., 2005; Pinu; Silva and Northen, 2015; Villas-Boas, 2017). Depending on the exometabolite produced, these molecules can mediate interspecies interactions that range from competitive to cooperative (Großkopf and Soyer, 2014). Of these interaction types, competition has been shown to have a major influence in structuring microbial communities (e.g., Foster and Bell, 2012; Coyte et al., 2015; Hibbing et al. 2010). Thus, competitive interactions that are mediated by exometabolites are also expected to influence to microbial community dynamics. In addition, different types of

exometabolites can be employed by bacteria to gain advantage in both exploitative (e.g. nutrient scavenging) and interference (direct cell damage) categories of competition.

Traditionally, competition has been viewed through the lens of resource acquisition (Tilman, 1986). In these studies, competitiveness is modeled with respect to yield given resource consumption and growth (Stewart and Levin, 1973; Smith, 2011). However, competition for *survival* or *maintenance* may be just as important as competition for yield, especially during periods of resource limitation (Pekkonen et al., 2011; Holt, 2008). Competition during maintenance is likely common in some free-living environments, such as soils, sequencing batch reactors, and the human gut that experience long periods of nutrient famine punctuated by short periods of nutrient influx (Schimel, 2018; Chiesa et al., 1985; Fetissov, 2017; Hiltunen et al., 2008). The stationary phase of a bacterial growth curve falls within this context of growth cessation, and pulses of nutrients may be transiently available as cells die and lyse (necromass), while the total population size remains stagnant. Stationary phase is often coordinated with a metabolic shift to secondary metabolism (Navarro Llorens et al., 2010; Čihák et al., 2017). Therefore, an effective “maintenance” competitor may produce bioactive exometabolites, like antibiotics, which are often produced as a result of secondary metabolism. In particular, bacteria can activate biosynthetic gene clusters (BSGCs) to produce bioactive exometabolites (Medema et al., 2015). The activation of BSGCs is closely tied to stress responses, suggesting that bacteria can sense the stress of competition (Cornforth and Foster, 2013; Okada and Seyedsayamdost, 2017). While it is known that certain exometabolites can trigger BSGC upregulation and, more generally alter transcription (Goh et al., 2002), there is much to understand about the

outcomes of interspecies interactions for BSGCs in multi-member microbial communities.

Here, we build on our previous research to understand how exometabolite-mediated interactions among bacterial neighbors contribute to community outcomes in a simple, three-member community (Table 1). These three members are commonly associated with terrestrial environments (soils or plants) and were chosen because of reported (Chandler et al., 2012) and observed interspecies exometabolite interactions in the laboratory. We used a synthetic community ("SynCom") approach (De Roy et al., 2014) by applying our previously described transwell system (Chodkowski and Shade, 2017), which allowed for evaluation of "community goods" within a media reservoir that was shared among members. The members' populations were physically isolated by membrane filters at the bottom of each transwell, but could interact chemically via the reservoir. In our prior work, we investigated each member's exometabolites and transcription over stationary phase, and the objective was to understand monoculture responses (in minimal glucose media) before assembling the more complex 2- and 3-member communities. We found that each member in monoculture produced a variety of exometabolites in stationary phase, including bioactive molecules involved in competition (Chodkowski and Shade, 2020). In this work, we build to 2- and 3- member arrangements to ask: How do members interact via exometabolites in simple communities during maintenance (stationary phase), and what are the competitive strategies and outcomes of those interactions? What genetic pathways, molecules, and members drive the responses? Which outcomes in 3-member community are predicted by the 2-member communities, and which are "greater than the sum of its parts"?

111 We found that *B. thailandensis* had a major influence on the transcriptional
112 responses of both *C. violaceum* and *P. syringae*, and that this influence could be
113 attributed to an increase in both interference and exploitative competition strategies.
114 Furthermore, we observed non-additive transcriptional responses and exometabolite
115 production, particularly for *B. thailandensis* with respect to BSGCs. These findings show
116 that diverse competitive strategies can be deployed even when bacterial neighbors are
117 surviving rather than exponentially growing. Therefore, we suggest that contact-
118 independent, exometabolite-mediated interference and exploitation are important
119 competitive strategies in resource-limited environments and support the non-yield
120 outcome of maintenance.

121

122 Table 1. Bacterial members used in the synthetic community (SynCom) system.

Member	***Burkholderia thailandensis* E264**	***Chromobacterium violaceum* ATCC 31532**	***Pseudomonas syringae* pv. tomato DC3000**
Genome size (Mb)	6.72	4.76	6.54
Family	*Burkholderiaceae*	*Neisseriaceae*	*Pseudomonadaceae*
No. of CDSs[a]	5639	4393	5576
Chromosomes	2	1	1
Plasmids	0	0	2
Reference	Brett et al., 1998	Wells et al., 1982	Buell et al. 2003

123 [a]CDSs, Coding sequences.

124

125 # Results

126 *Stationary phase dynamics of microbial communities: transcriptional responses*

127 We had four replicate, independent timeseries of each of seven community
128 arrangements (three monocultures plus four cocultures of every pair and the 3-member
129 arrangement), and here focus on the coculture analyses to gain insights into community
130 outcomes. A range of 518 to 1204 genes were differentially expressed by each member
131 in coculture, irrespective of the identity of neighbors (Fig. S1.1, false discovery rate
132 adjusted p-value (FDR)≤ 0.01). In addition, each member also had differential gene
133 expression that was unique to a particular neighbor(s). Summarizing across all
134 coculture arrangements, 2,712/5639 (48.1%), coding sequences (CDSs), 3267/4393
135 CDSs (74.4%), and 4974/5576 CDSs (89.2%) genes in *B. thailandensis*, *C. violaceum*,
136 and *P. syringae* were differentially expressed, respectively (FDR≤0.01). Both community
137 membership and time contributed to the transcriptional response of each member (Fig.
138 1, Table S1.1). Together, these data suggest that there are both general and specific
139 consequences of neighbors for the transcriptional responses of these bacterial
140 community members.

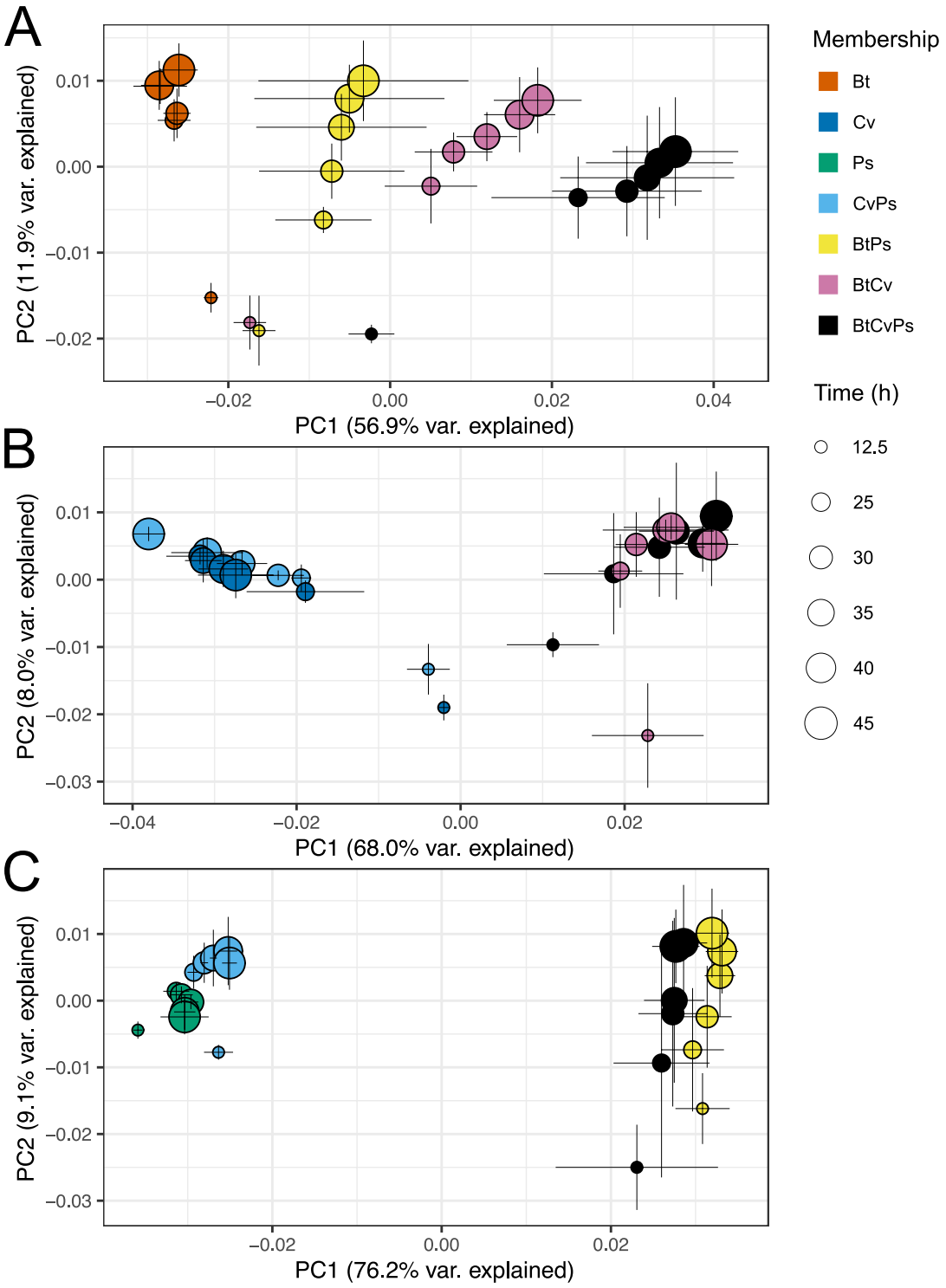

Figure 1. Transcriptional responses are driven by community membership and time. Shown are principal coordinates analysis (PCoA) plots for *B. thailandensis* (Bt, A), *C. violaceum* (Cv, B), and *P. syringae* (Ps, C). Each point represents a mean transcript profile for a community member given a particular community arrangement (neighbor(s) included, indicated by symbol color) and sampled at a given time point over exponential and stationary growth phases (in hours since inoculation, h, indicated by symbol size, n=3 to 4 replicates per timepoint/community arrangement). The Bray-Curtis distance

metric was used to calculate dissimilarities between transcript profiles. Error bars are 1 standard deviation around the mean axis scores.

Temporal trajectories in transcript profiles were generally reproducible across replicates for each member given a particular community arrangement (PROTEST analyses, Table S1.2). Each member had a distinct transcript profile ($0.480 \leq r2 \leq 0.778$ by Adonis; P value, 0.001; all pairwise false discovery rate [FDR]-adjusted P values, ≤0.068 except for the *C. violaceum* coculture with *B. thailandensis* vs 3-member comparison, Table S1.3). For all ordinations, community membership had the most explanatory value (Axis 1), followed by time (Axis 2), with the most variation explained by the interaction between time and membership (Table S1.1). Membership alone accounted for 60.6% and 77.0% of the variation explained in *C. violaceum* and *P. syringae* analyses, respectively and 46.3% in the *B. thailandensis* analysis (Table S1.3).

When included in the community, *B. thailandensis* strongly determined the transcript profiles of the other two members. For example, the inclusion of *B. thailandensis* in a coculture differentiated transcript profiles for both *C. violaceum* and *P. syringae* (Fig. 1B & 1C). Thus, *B. thailandensis* appears to have had a dominating influence on the transcriptional response of neighbors, and these responses were dynamic with respect to time.

We analyzed clusters of orthologous groups of proteins (COGs) to infer the responses of members to their neighbors. Differentially expressed genes were categorized as upregulated or downregulated based on temporal patterns and representation in COG groups (Fig. S1.2). We focused on the largest discrepancies

171 between upregulated and downregulated within COG groups, which provide insights
172 into broad biological processes affected by exometabolite interactions. COG groups
173 trending towards upregulation in *B. thailandensis* included secondary metabolites
174 biosynthesis, transport, and catabolism [Q], signal transduction mechanisms [T], and
175 cell motility [N] while COG categories trending towards downregulation included cell
176 cycle control, cell division, chromosome partitioning [D], translation, ribosomal structure
177 and biogenesis [J], and defense mechanisms [V]. These results suggest that *B.*
178 *thailandensis* responds to neighbors via downregulation of growth and reproduction and
179 upregulation of secondary metabolism. We therefore hypothesized that *B. thailandensis*
180 was producing bioactive exometabolites against *C. violaceum* and *P. syringae* to
181 competitively inhibit their growth.

182 Because of the strong transcript response of *C. violaceum* and *P. syringae* when
183 neighbored with *B. thailandensis* (Fig. 1B & 1C), we first focused on COG group trends
184 within community arrangements with *B. thailandensis* (Fig. S1.2B & S1.2C, rows 2 & 3).
185 COG groups tending towards upregulation in *C. violaceum* and *P. syringae* were
186 translation, ribosomal structure and biogenesis [J] and replication, recombination, and
187 repair [L], respectively. COG groups tending towards downregulation in *C. violaceum*
188 and *P. syringae* were signal transduction mechanisms [T] and secondary metabolites
189 biosynthesis, transport, and catabolism [Q], respectively. These results suggest that the
190 presence of *B. thailandensis* alters its neighbor's ability to respond to the environment
191 and inhibits secondary metabolism.

192 We were interested in understanding patterns of differential gene regulation and
193 how individual genes contribute to the observed dynamics in Figure 1. The top ~500

194 differentially expressed genes (see methods: *Circos plots*) were visualized by genomic
195 location and temporal dynamics (Figs. S1.3-S1.5). These results show that the gene
196 dynamics for *C. violaceum* and *P. syringae* when grown in the 3-member community
197 are consistent with each neighbor's gene dynamics when grown only with *B.*
198 *thailandensis* (Figs. S1.4 & S1.5, heatmap, outer two tracks vs. inner two tracks).
199 Interestingly, 68.4% (340 genes) of the top differentially regulated genes in *B.*
200 *thailandensis* were located on chromosome II despite chromosome II only accounting
201 for 44.0% of all coding sequences (2365 coding sequences). In addition, nearly all *P.*
202 *syringae* plasmid genes were upregulated when *P. syringae* was neighbored with *B.*
203 *thailandensis*. These plasmids were significantly enriched for processes related to DNA
204 recombination, recombinase activity, and DNA binding/integration (GO enrichment,
205 Table S1.4).

206

207 *Stationary phase dynamics of microbial communities: exometabolomic responses*

208 Because member populations are physically separated in the SynCom transwell
209 system but allowed to interact chemically, observed transcript responses in different
210 community arrangements are inferred to result from exometabolite interactions. Spent
211 medium from the shared medium reservoir was collected from each transwell plate and
212 analyzed using mass spectrometry to detect exometabolites. We focused our analysis
213 on those exometabolites that had maximum accumulation in a coculture community
214 arrangement (either in pairs or in 3-member community). Consistent with the transcript
215 analysis, we found that both community membership and time explained the

exometabolite dynamics, and that the explanatory value of membership and time was maintained across all polarities and ionization modes (Fig. 2, Table S2.1).

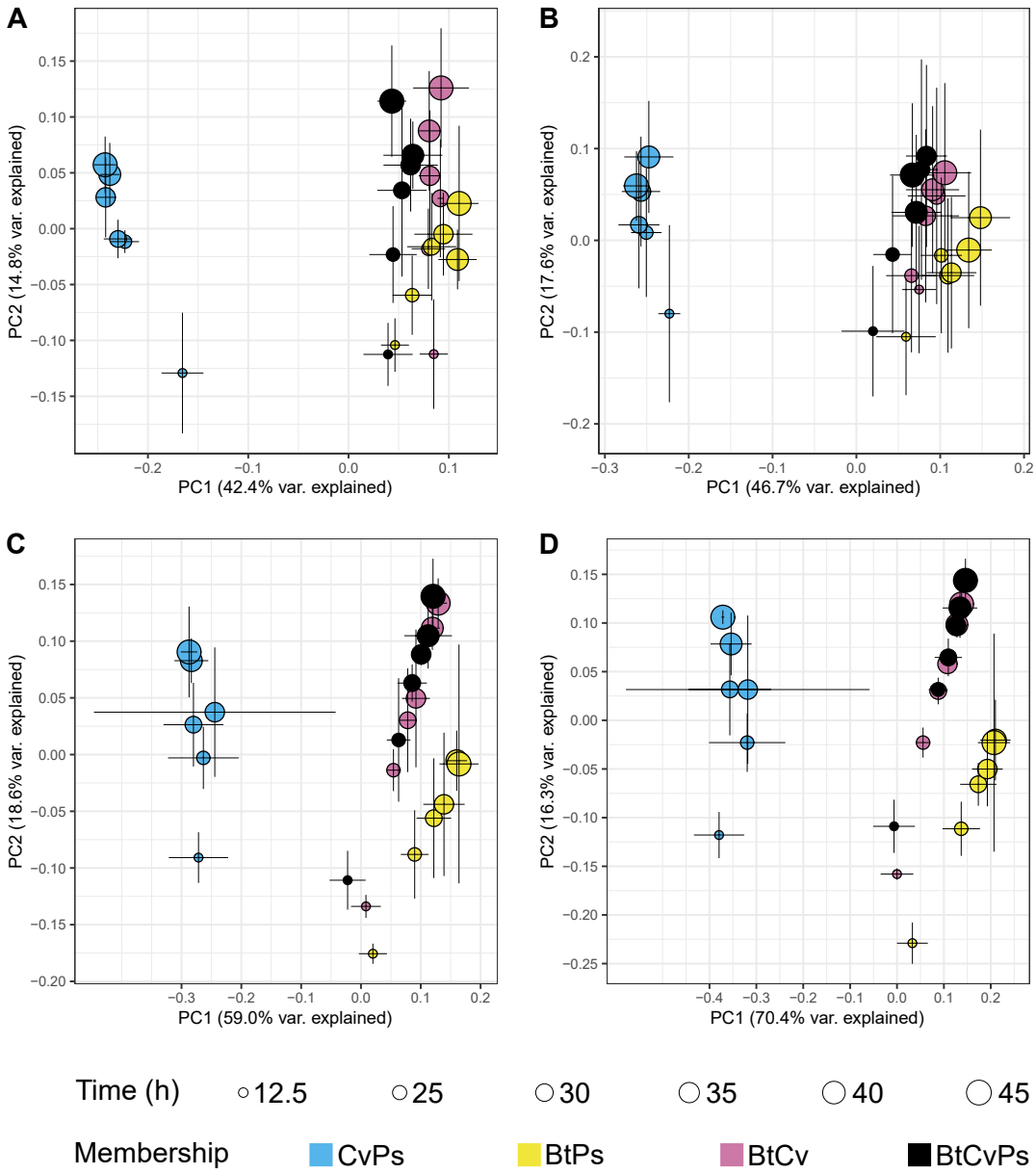

Figure 2. Bacterial community exometabolite profiles differ by community membership and time. Shown are PCoA plots for exometabolite profiles from the following mass spectrometry modes: polar positive (A), polar negative (B), nonpolar positive (C), and nonpolar negative (D). Each point represents the mean exometabolite profile (relative contributions by peak area) given a particular community membership (indicated by symbol color) at a particular time point (indicated by symbol shape). The Bray-Curtis distance metric was used to calculate dissimilarities between exometabolite profiles. Error bars are

1 standard deviation around the mean axis scores (n= 2 to 4 replicates). Bt is *B. thailandensis*, Cv is *C. violaceum*, and Ps is *P. syringae*.

Temporal trajectories in exometabolite profiles were generally reproducible across replicates with some exceptions (PROTEST analyses, Table S2.2, Supplementary File 2.1). Exometabolite profiles were distinct by community membership ($0.475 \leq r2 \leq 0.662$ by Adonis; P value, 0.001; all pairwise false discovery rate [FDR]-adjusted P values, ≤0.025, Table S2.3), and also dynamic over time. As observed for the member transcript profiles, and the interaction between membership and time had the highest explanatory value for the exometabolite data (Table S2.1).

We found that the *C. violaceum-P. syringae* coculture exometabolite profiles were consistently the most distinct from the other coculture memberships (Fig. 2), supporting, again, that the inclusion of *B. thailandensis* was a major driver of exometabolite dynamics, possibly because it provided the largest or most distinctive contributions to the community exometabolite pool. Indeed, we observed that a majority of the most abundant exometabolites were either detected uniquely in the *B. thailandensis* monoculture or accumulated substantially in its included community arrangements (Fig. S2.1). Some exometabolites detected in *B. thailandensis*-inclusive communities were not detected in its monocultures (Fig. S2.1D), suggesting that the inclusion of neighbors contributed to the accumulation of these particular exometabolites (e.g. upregulation of biosynthetic gene clusters or lysis products). *C. violaceum* and *P. syringae* contributed less to the 3-member community exometabolite profile, as exometabolites detected in the *C. violaceum-P. syringae* coculture arrangement were less abundant and had lower accumulation over time in the 3-

member community arrangement (Fig. S2.1A). Together, these results suggest that *B. thailandensis* can suppress or overwhelm expected outputs from neighbors.

In summary, we observed both increased accumulation and unique production of exometabolites in pairwise cocultures and in the 3-member community arrangements, with *B. thailandensis* contributing the most to the shared exometabolite pool as determined by comparisons with its monoculture exometabolite profile. Related, the transcriptional responses of *C. violaceum* and *P. syringae* in the 3-member community arrangement is most similar to their respective transcriptional response when neighbored with *B. thailandensis* alone, despite the presence of the third neighbor.

B. thailandensis increases competition strategies in the presence of neighbors

We observed relatively unchanged viability in *B. thailandensis* (Fig. S3.1). On the contrary, we observed a slight reduction (~2.1 log2 fold change) in *C. violaceum* live cell counts, and a drastic reduction (~4.7 log2 fold change) in *P. syringae* live cell counts, when either was cocultured with *B. thailandensis* (Figs. S3.2 & S3.3). Given this reduction in viability and that there have been competitive interactions between *B. thailandensis* and *C. violaceum* previously reported (Chandler et al., 2012), we hypothesized that *B thailandensis* was using competition strategies to influence its neighbors via production of bioactive exometabolites. If true, we would expect an upregulation in *B. thailandensis* biosynthetic gene clusters (BSGC) that encode bioactive exometabolites. Indeed, we found evidence of this when *B. thailandensis* had neighbors (Fig. 3, Table S3.1).

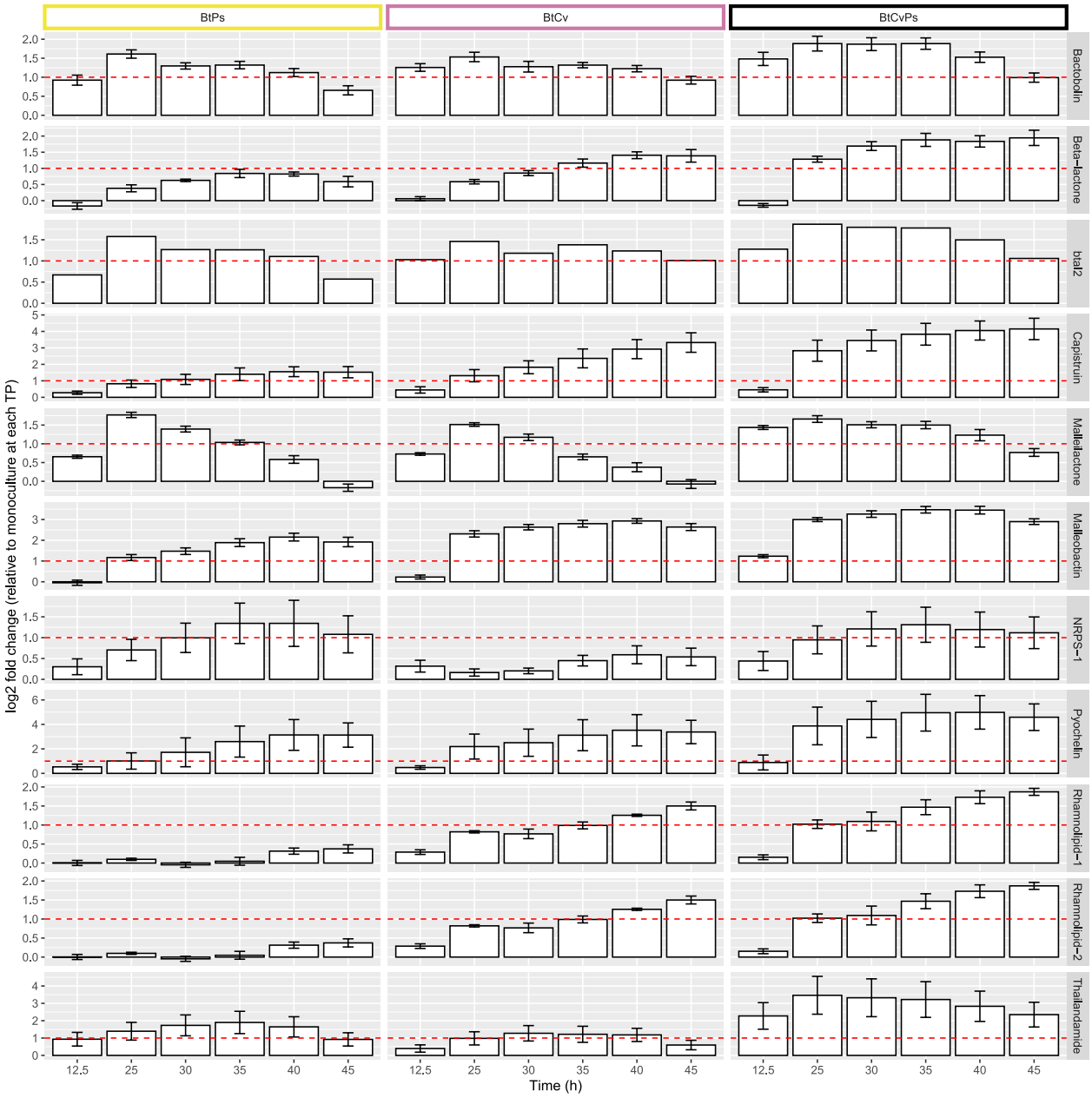

271

272 **Figure 3. *B. thailandensis* upregulates biosynthetic gene clusters (BSGC) in cocultures.** Columns
273 represent community membership where Bt: *B. thailandensis*, Cv: *C. violaceum*, and Ps: *P. syringae* and
274 rows represent BSCC in *B. thailandensis*. Genes part of a BSGC were curated from antiSMASH
275 predictions and literature-based evidence. Within each BSGC, log2 fold-changes (LFC) were calculated
276 by comparing gene counts from a coculture to the monoculture control at each time point. LFC were then
277 averaged from all biosynthetic genes in the BSGC at each time point. We defined an upregulated BSGC
278 as a BSGC that had at least two consecutive stationary phase time points with a LFC > 1 (indicated by
279 the horizontal line). Note that plots for each BSGC have separate scales for the Y-axis.

280

281 This suggests that *B. thailandensis* responded to neighbors by upregulating
282 genes involved in the production of bioactive compounds, likely to gain a competitive
283 advantage. However, not all BSGCs in *B. thailandensis* were upregulated. Some
284 BSGCs were unaltered or downregulated (Fig. S3.4). *C. violaceum* upregulated only 1
285 BSGC in coculture with *B. thailandensis,* while *P. syringae* did not upregulate any
286 BSGC in any coculture (Figs. S3.5 & S3.6). Interestingly, coculturing with *C. violaceum*
287 and *P. syringae* resulted in the upregulation of an unidentified beta-lactone and an
288 unidentified non-ribosomal peptide synthetase (NRPS) in *B. thailandensis*, respectively.
289 Similarly, coculturing with *B. thailandensis* resulted in the upregulation on an
290 unidentified NRPS- Type I polyketide synthase in *C. violaceum*. We also note that two
291 additional unidentified NRPS passed the LFC threshold of 1 in *C. violaceum*. However,
292 these were only upregulated at the exponential phase time point and subsequently
293 downregulated or below the LFC threshold in all stationary phase time points.
294 Interspecies interactions led to the upregulation of BSGC in both *B. thailandensis* and
295 *C. violaceum* and three of these BSGC encode potentially novel bioactive
296 exometabolites.

297 We were able to identify 6 of the 11 products from the upregulated *B.*
298 *thailandensis* BSGC and quantify their abundances from mass spectrometry data (Fig.
299 S3.7, Table S3.2). For any given identified exometabolite, it differentially accumulated
300 between community arrangements containing *B. thailandensis* (Table S3.3), particularly
301 when comparing the *B. thailandensis* monoculture compared to each coculture
302 arrangement (Table S3.4). As expected, these identified exometabolites were not
303 detected in community arrangements that did not include *B. thailandensis*. Bactobolin

304 was the only identified exometabolite that accumulated in monoculture to equivalent
305 levels of accumulation in all coculture conditions. Thus, *B. thailandensis* increased
306 competition strategies with neighbors through the upregulation and production of many
307 bioactive exometabolites. Of these bioactive exometabolites, three are documented
308 antimicrobials (Amunts et al., 2015; Kuznedelov et al., 2011; Wozniak et al., 2018), two
309 are siderophores (Biggins et al., 2012; Butt and Thomas, 2017), and one is a
310 biosurfactant (Dubeau et al., 2009). We conclude that *B. thailandensis* produced
311 bioactive exometabolites to competitively interact using both interference and
312 exploitative competition strategies (Ghoul and Mitri, 2016). Given that *B. thailandensis*
313 upregulated competition strategies, and responded more broadly in producing
314 competition-supportive exometabolites when grown with neighbors, we hypothesized
315 that these bioactive exometabolites are responsible for the altered transcriptional
316 responses in *C. violaceum* and *P. syringae*.

317

318 *Interspecies co-transcriptional networks reveal coordinated gene expression related to*
319 *competition*

320 We performed interspecies coexpression network analysis to infer interspecies
321 interactions. We used temporal profiles to generate 23 and 24 coexpression networks
322 for *B. thailandensis-C. violaceum* and *B. thailandensis-P. syringae* cocultures,
323 respectively (Table S4.1). As expected, the majority of nodes network had intraspecies
324 edges only, with interspecies edges comprising 1.85% and 1.90% of the total edges in
325 the *B. thailandensis-C. violaceum* and *B. thailandensis-P. syringae* networks,

respectively. We explored interspecies edges for evidence of interspecies transcriptional co-regulation.

We performed two analyses (module analysis and GO enrichment) to validate networks and infer interspecies interactions (Fig. S4.1). Module analysis validated networks as intraspecies modules enriched for biological processes (Supplementary File 4.1). To infer interspecies interactions, we filtered genes with interspecies edges and performed enrichment analysis (Supplementary File 4.2). The top enriched Gene Ontology (GO) term for *B. thailandensis* when paired with *C. violaceum* was antibiotic synthesis of thailandamide, supporting interference competition. Though the top enriched GO term in *B. thailandensis* when paired with *P. syringae* was bacterial-type flagellum-dependent cell motility, antibiotic synthesis of malleilactone was also enriched. Both thailandamide genes from the *B. thailandensis*-*C. violaceum* network (Fig. 4) and malleilactone genes from the *B. thailandensis*-*P. syringae* network (Fig. S4.2) formed near-complete modules within their respective BSGCs.

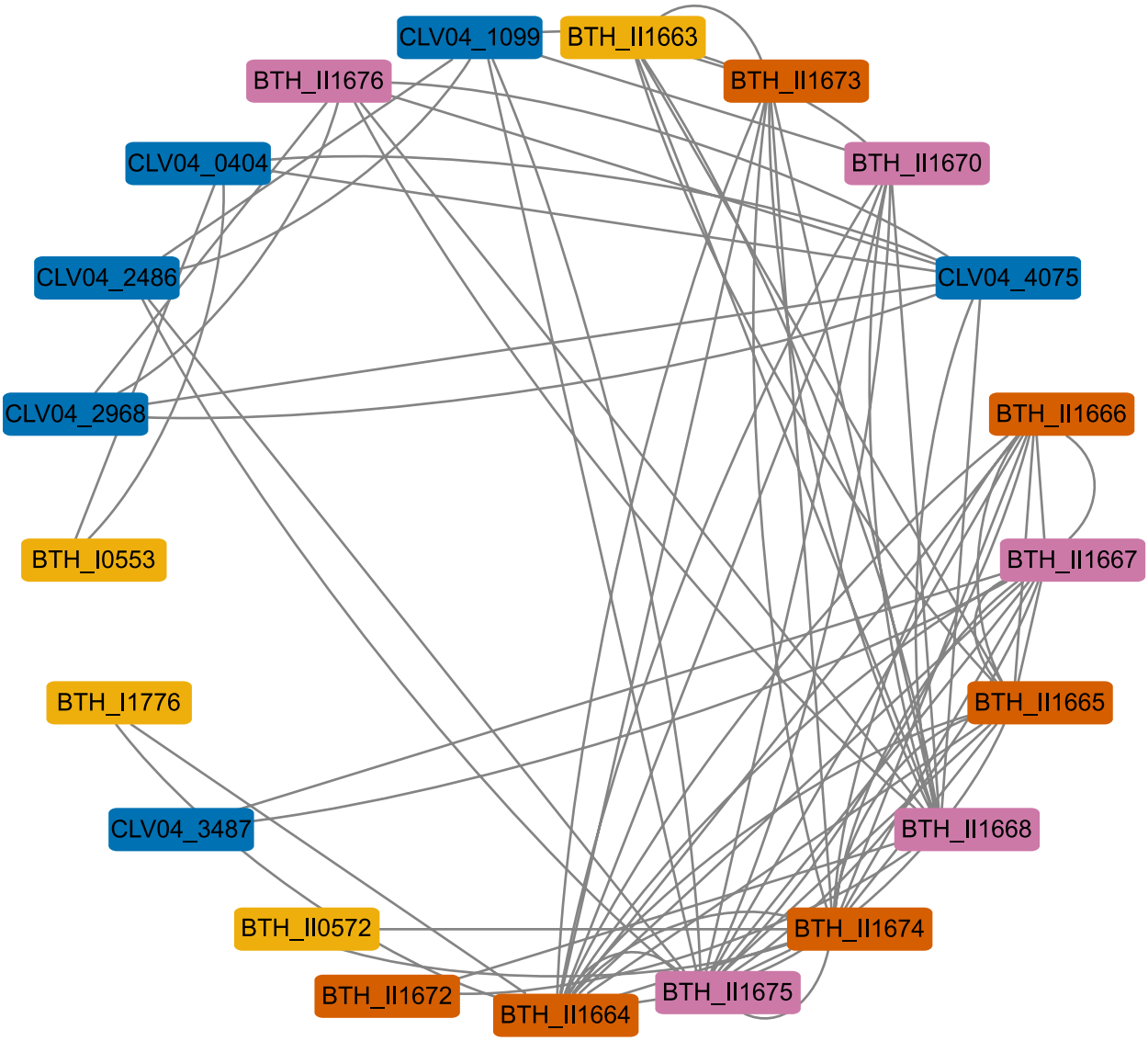

340

	B. thailandensis-C. violaceum interspecies network	*B. thailandensis-P. syringae* interspecies network
Bactobolin	✓	✓
Beta-lactone	✓	×
Capistruin	✓	✓
Malleilactone	✓	✓
Malleobactin	✓	✓
NRPS-1	×	✓
Pyochelin	✓	✓
Rhamnolipid	×	×
Thailandamide	✓	✓

341

342 **Figure 4. *B. thailandensis* genes involved in thailandamide production are detected as**
343 **interspecies edges in the *B. thailandensis*-*C. violaceum* coexpression network and biosynthetic**
344 **genes organize into network modules.** A network module containing the thailandamide BSGC is
345 shown. The network module nodes are color coded by *B. thailandensis* gene type (BSGC or not) and type
346 of connections (interspecies or not): thailandamide biosynthetic genes that had interspecies edges
347 (magenta), thailandamide biosynthetic genes that did not have interspecies edges (orange), or other
348 genes that were not part of the BSGC (yellow); as well as genes that were from *C. violaceum* (blue). The
349 chromosomal organization of the thailandamide BSGC is shown below the network module. The same
350 colors are applied to the BSGC operon. The operons also depict genes that were not detected within the
351 interspecies network, shown in gray. Asterisks indicate core biosynthetic genes in the BSGCs, as
352 predicted from antiSMASH. The table shows upregulated *B. thailandensis* BSGCs (Fig. 3) and whether
353 there were interspecies edges detected (check is yes, x is no).

354

355 At least one gene from each of *B. thailandensis's* upregulated BSGCs (Fig. 3, Table)
356 had an interspecies edge, except for rhamnolipid. The top GO term for both *C.*
357 *violaceum* and *P. syringae* genes that had edges shared *B. thailandensis* was bacterial-
358 type flagellum-dependent motility. Other notable enriched GO processes were efflux
359 activity for *C. violaceum* and signal transduction for *P. syringae*. Specifically, a DNA
360 starvation/stationary phase gene (CLV04_2968, Fig. 4), *dspA*, was connected within the
361 thailandamide module of the *B. thailandensis*-*C. violaceum* network and a TonB-
362 dependent siderophore receptor gene (PSPTO_1206, Fig. S4.2) was connected within
363 the malleilactone module of the *B. thailandensis*-*P. syringae* network (Supplementary
364 File 4.3). Interestingly, both CLV04_2968 and PSPTO_1206 were differentially
365 downregulated when cocultured with *B. thailandensis* (Figs. S4.3A & S4.4A,
366 respectively). Additionally, the closest homolog for *dspA* in *B. thailandensis* was
367 unaltered (BTH_I1284, Supplementary File 4.4) when cocultured with *C. violaceum* (Fig.
368 S4.3B) and the closest homolog to the TonB-dependent receptor in *B. thailandensis*
369 (BTH_I2415, Supplementary File 4.5) was differentially upregulated when cocultured
370 with *P. syrinage* (Fig. S4.4B). Taken together, these interspecies networks revealed that
371 *B. thailandensis* BSGC have coordinated expression patterns to biological process in

372 both *C. violaceum* and *P. syringae*, suggesting that bioactive exometabolites were
373 driving their transcriptional responses.

374

375 *Distinctive member responses when assembled together*

376 Within a complex community, there can be outcomes that are not expected
377 based on interactions that are observed in simpler situations of member pairs (Sanchez-
378 Gorostiaga et al., 2019; Mickalide et al., 2019; D'hoe et al., 2018). A typical predictive
379 approach uses the additivity assumption, where the null expectation is that a members'
380 outcome in more complex communities is a summation of its outcomes in simpler
381 communities (Momeni et al., 2017). Patterns that deviate from the assumption arise
382 from biological phenomena that are deemed non-additive. Much emphasis has been
383 placed on predictions on the additive (or non-additive deviation) nature of growth
384 outcomes in more complex environments (Foster and Bell, 2012; Pacheco et al., 2021;
385 Estrela et al., 2021). Here, we evaluated non-additive responses (e.g. transcriptomics)
386 and behaviors (e.g. exometabolite production). We identified genes with non-additive
387 upregulation in the 3-member community (Fig. S5.1, Supplementary File 5.1, see
388 methods: *Non-additive gene expression*). For *B. thailandensis*, most of these genes
389 consistently had nonadditive upregulation throughout stationary phase. Both *P. syringae*
390 and *C. violaceum* trended towards transient dynamics of non-additive upregulation,
391 which tended to occur at a specific timepoint. For each member, there was a stark
392 contrast in genes with non-additivity between the exponential phase timepoint and all
393 stationary phase time points. Notably, the top GO enrichments included antibiotic
394 biosynthesis for *B. thailandensis* and structural constituents of the ribosome for both *C.*

395 *violaceum* and *P. syringae* (Supplementary File 5.2). Of the BSGC in *B. thailandensis*,
396 multiple genes involved in the production of thailandamide, pyochelin, capistruin, and
397 malleobactin had non-additive upregulation. Since we were able to identify some of
398 these compounds as features within the mass spectral data, we asked if non-additive
399 transcriptional activity corresponded to non-additive exometabolite production.

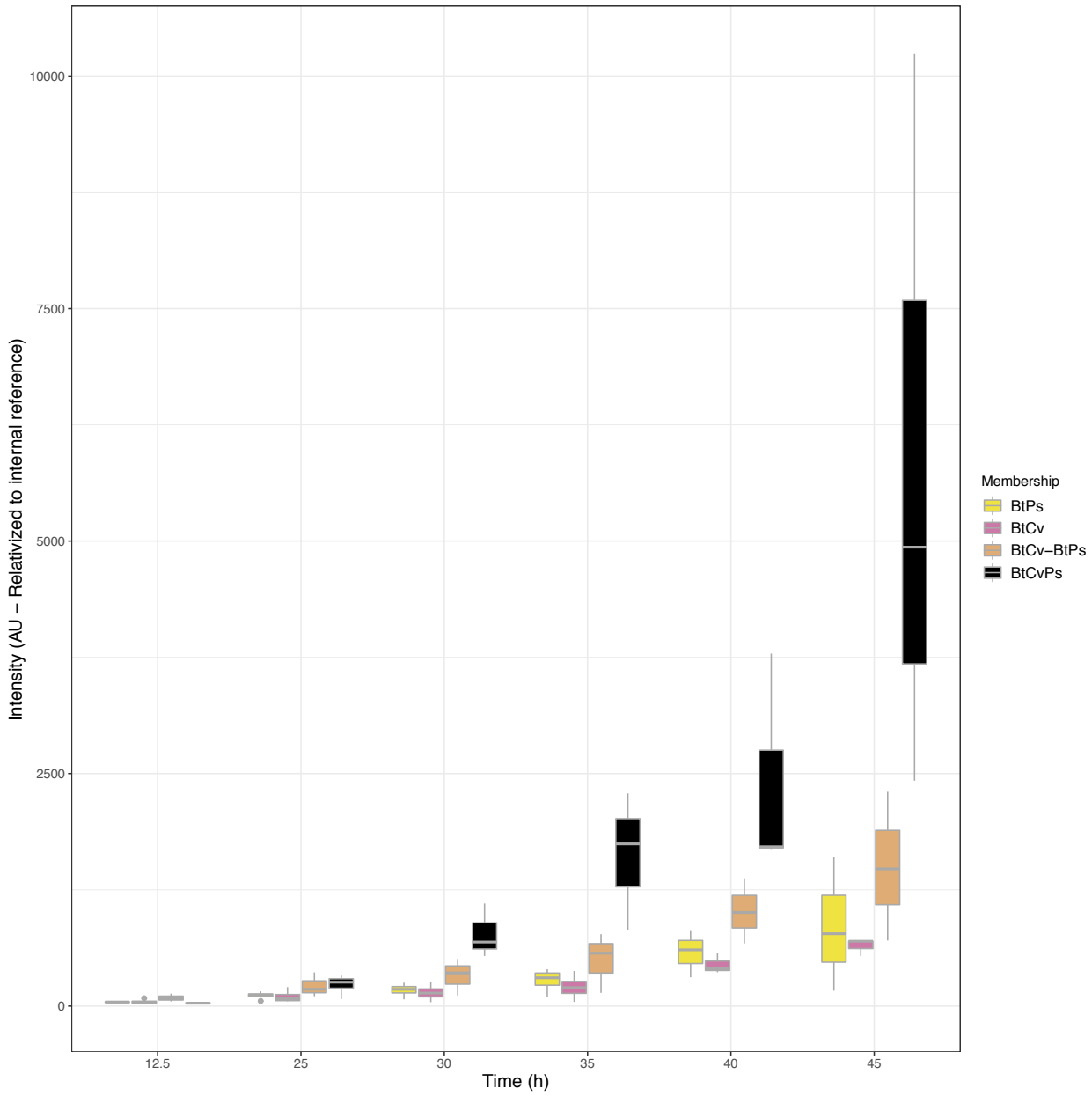

400

401 **Figure 5. Thailandamide accumulates in a non-additive manner**. The accumulation of thailandamide
402 was quantified through time (*n* = 3-4 integrated peak areas per time point). The bottom and top of the box
403 are the first and third quartiles, respectively, and the line inside the box is the median. The whiskers
404 extend from their respective hinges to the largest value (top), and smallest value (bottom) was no further
405 away than 1.5× the interquartile range. Colors correspond to the community membership for the
406 *B.thailandensis-P. syringae* coculture (yellow, BtPs), the *B. thailandensis-C, violaceum* coculture
407 (magenta, BtCv), the "expected" exometabolite abundance in the 3-member community obtained from
408 additive peak areas from the *B.thailandensis-P. syringae* and *B.thailandensis-C, violaceum* cocultures
409 (orange, BtCv+BtPs), and the 3-member community (black, BtCvPs).

410

411

412 Most exometabolite features did not exceed expectations of additivity, as the average
413 fold change across all time points was ~0.6 (Fig. S5.2). However, we did find that 858
414 exometabolomic features accumulated in the 3-member community in a non-additive
415 manner (Fig. S5.3), including thailandamide (Fig. 5) and pyochelin (Fig. S5.4), but not
416 capistruin (Fig. S5.5). At the final stationary phase time point (45 h), thailandamide
417 accumulated ~4-fold more and pyochelin accumulated ~3-fold more than the additive
418 expectation. Thailandamide and pyochelin were consistently above 1σ of the average
419 additive fold change for all coculture filtered exometabolites throughout stationary phase
420 (Fig. S5.2, ablines). We combined peak areas from pairwise cocultures to create an
421 "expected" exometabolite abundance over the time course for thailandamide, pyochelin,
422 and capistruin (Figs. 5, S5.4, S5.5, orange). The experimental exometabolite
423 abundance over the time course was significantly different from the "expected"
424 exometabolite abundance for thailandamide, but not for pyochelin and capistruin
425 (repeated measures ANOVA, Table S5.1). When comparing each time point separately
426 for thailandamide, significance was obtained only for the initial time point, and later time
427 points were trending toward significance (Table S5.2).

Discussion

Here, we used a synthetic community system to understand how exometabolomic interactions determine members responses and behaviors. Our experiment used a bottom-up approach to compare the seven possible community arrangements of three members, and their dynamics in member transcripts and community exometabolites over stationary phase. Differential gene expression across community arrangements and over time show that the exometabolites released by a member were sensed and responded to by its neighbors. Furthermore, members' behaviors in monocultures changed because of coculturing, as evidenced by differential exometabolite production. *B. thailandensis* evoked the largest transcriptional changes in *C. violaceum* and *P. syringae*, and these changes were driven largely by several increases in *B. thailandensis* competitive strategies. Numerous transcripts and exometabolite were non-additive in the 3-member community, suggesting that predictions of members outcomes in more complex communities will not always be a simple summation of pairwise outcomes. That interactions within a relatively simple community altered the behavior of each member is important because these kinds of behavioral changes could, in turn, drive changes in community structure and/or function in an environmental setting. For example, it was shown that interspecies interactions more strongly influenced the assembly of *C. elegans* gut communities than host-associated factors (Ortiz et al., 2021). Therefore, mechanistic and ecological characterization of interspecies interactions will inform as to the principles that govern emergent properties of microbial communities.

451 Overall, competitive interactions predominated in this synthetic community. Our
452 previous study found that, over stationary phase in monocultures, each member
453 released and accumulated at least one exometabolite documented to be involved in
454 either interference or exploitative competition (Chodkowski and Shade, 2020). This
455 suggests that entry into stationary phase primed members for competitive interactions,
456 whether there were heterospecific neighbors present. We interpret this strategy of
457 preemptive aggression to be especially advantageous to *B. thailandensis,* as it
458 successfully used competitive strategies against both *C. violaceum* and *P. syringae*. *B.*
459 *thailandensis's* success was supported by decreased viable *P. syringae* cells when
460 cocultured with *B. thailandensis*. Though *C. violaceum* viable cell counts were not as
461 affected directly by the coculture with *B. thailandensis*, *B. thailandensis*-produced
462 bactobolin (Duerkop et al., 2009) was detected in the shared medium reservoir.
463 Bactobolin is a bacteriostatic antibiotic previously shown to be bioactive against *C.*
464 *violaceum* (Chandler et al., 2012). But, *C. violaceum* can resist bactobolin through
465 upregulation of an RND-type efflux pump (Evans et al., 2018). This finding also is
466 supported by our data, as all genes coding for the CdeAB-OprM RND-type efflux
467 system and the TetR-family transcriptional regulator were upregulated in *C. violaceum*
468 cocultures with *B. thailandensis* (CLV04_2412-CLV04_2415).

469 Coculturing can induce secondary metabolism (Pettit, 2009; Netzker et al., 2015;
470 Zhu et al., 2014) because an exometabolite produced by one microbe can prompt
471 secondary metabolism in a neighbor (Okada and Seyedsayamdost, 2017). We found
472 that coculturing led to the upregulation of numerous BSGCs in *B. thailandensis*. These
473 exometabolites included bactobolin, malleilactone (Biggins et al., 2012; Truong et al.,

474 2015; siderophore and cytotoxin), malleobactin (Alice et al., 2006; Gupta et al., 2017;
475 siderophore), capistruin (Knappe et al., 2008; lasso peptide), thailandamide (Ishida et
476 al., 2010; polyketide), pyochelin (Butt and Thomas, 2017; siderophore), rhamnolipids
477 (Dubeau et al., 2009; biosurfactants), and two uncharacterized BSGCs encoding
478 nonribosomal peptide synthetases. Of these exometabolites, bactobolin, capistruin, and
479 thailandamide have documented antimicrobial activities through translation inhibition
480 (Amunts et al., 2015), transcription inhibition (Kuznedelov et al., 2011), and inhibition of
481 fatty acid synthesis (Wozniak et al., 2018), respectively. For those exometabolites we
482 were able to identify with mass spectrometry, their accumulation in cocultures was
483 correlated with the upregulation of their BSGCs. Furthermore, up/downregulated
484 patterns across all *B. thailandensis* BSGCs is consistent with ScmR global regulatory
485 patterns of secondary metabolism (Mao et al., 2017). Though we were not able to
486 pinpoint the exact inducers of BSGCs, exometabolites such as antibiotics (Okada et al.,
487 2016) and primary metabolites (Li et al., 2020) have been documented to induce
488 secondary metabolism in *B. thailandensis*. *C. violaceum* can inhibit *B. thailandensis*
489 (Chandler et al., 2012) but we did not observe *B. thailandensis* inhibition based on cell
490 counts. However, we did find that in stationary phase *C. violaceum*-*B. thailandensis*
491 cocultures, *C. violaceum* upregulated an uncharacterized hybrid nonribosomal peptide
492 synthetase-type I polyketide synthase. *P. syringae* was the least competitive of the
493 three neighbors, as evidenced by a reduction in live cell counts when cocultured with *B.*
494 *thailandensis*. Also, *P. syringae* did not increase competitive strategies when
495 cocultured, as no BSGCs were consistently upregulated across all coculture conditions.
496 In summary, though all three neighbors used competitive strategies, *B. thailandensis*

497 was most successful and displayed continued aggression in cocultures over stationary
498 phase through increased production of exometabolites involved in interference and
499 exploitative competition strategies.

500 Given the upregulation of BSGCs in *B. thailandensis* and the strong
501 transcriptional responses of *C. violaceum* and *P. syringae* to the presence of *B.*
502 *thailandensis*, we hypothesized that competitive exometabolites were contributing to
503 their community dynamics. Thus, we used a coexpression network analysis with our
504 longitudinal transcriptome series to infer interspecies interactions (McClure, 2019). This
505 use of this approach was first demonstrated to infer coregulation between a phototroph-
506 heterotroph commensal pair (McClure et al., 2018). Our network confirmed that *B.*
507 *thailandensis* BSGCs had coordinated gene expression patterns with both *C. violaceum*
508 and *P. syringae*. Interspecies nodes in both networks contained various genes involved
509 in the aforementioned upregulated *B. thailandensis* BSGCs. In particular, we focused on
510 interspecies edges within thailandamide nodes for the *B. thailandensis*-*C. violaceum*
511 network and interspecies edges within malleilactone nodes for the *B. thailandensis*-*P.*
512 *syringae* network because these were significantly enriched as interspecies nodes. A *C.*
513 *violaceum* gene of interest, CLV04_2968, was contained within the thailandamide
514 cluster of interspecies nodes. This gene codes for a DNA starvation/stationary phase
515 protection protein and had the highest homology to the Dps protein in *Escherichia coli*
516 across all *C. violaceum* protein coding genes. Dps mediates tolerance to multiple
517 stressors and *dps* knockouts are more susceptible to thermal, oxidative, antibiotic, iron
518 toxicity, osmotic, and starvation stressors (Karas et al., 2015). Interestingly,
519 CLV04_2968 was downregulated when cocultured with *B. thailandensis*, suggesting

520 that *B. thailandensis* attenuates *C. violaceum* stress tolerance over stationary phase.
521 While we observed a slight decrease in viable *C. violaceum* cells when cocultured with
522 *B. thailandensis*, one may expect *C. violaceum* to have increased sensitivity to a
523 subsequent stress (e.g. pH stress; Nair and Finkel, 2004) resulting from CLV04_2968
524 downregulation in the presence of *B. thailandensis*.

525 In the *B. thailandensis*-*P. syringae* coexpression network, a *P. syringae* gene of
526 interest, PSPTO_1206, was contained within the malleilactone cluster of interspecies
527 nodes. PSPTO_1206 is annotated as a TonB-dependent siderophore receptor. A *P.*
528 *syringae* iron-acquistion receptor had coordinated expression with a malleilactone,
529 which has been characterized as a siderophore with antimicrobial properties (Biggins et
530 al., 2012). Interestingly, this gene was downregulated when in coculture with *B.*
531 *thailandensis*. In contrast, the closest TonB-dependent siderophore receptor homolog to
532 PSPTO_1206 in *B. thailandensis*, BTH_I2415, was upregulated in coculture conditions
533 with *P. syringae*. To summarize, coexpression network analysis reveal coordinated
534 gene expression patterns that helped to infer that BSGC upregulation likely explains the
535 influence of *B. thailandensis* on both *C. violaceum* and *P. syringae. B. thailandensis*-
536 increased competition strategies were coordinated with a potential decrease in
537 competition strategies in *C. violaceum* via reduced stress tolerance and in *P. syringae*
538 with reduced iron acquisition ability.

539 A major goal in microbial ecology is to predict community dynamics for purposes
540 of modulating and/or maintaining ecosystem function (Antwis et al., 2017, Konopka,
541 2009). At its core, microbial functional properties emerge, in part, from the concerted
542 interactions of multi-species assemblages. Predictions can be complicated by non-

additive phenomena that arise in more complex communities. For example, non-additive phenomena have been documented in gene expression (Cornforth et al., 2014; Bundy et al., 2002), growth (Pacheco et al., 2021), and fitness (Morin et al., 2018). Here, we also have documented non-additive responses and behaviors in our system when combinatorial stimuli were present in the 3-member community. *B. thailandensis* BSGCs displayed non-additive phenomena, as we are able show that the transcriptional response of certain BSGCs in the 3-member community was greater than the naive summation of transcriptional response in pairwise arrangements. Furthermore, non-additive transcriptional responses resulted in non-additive exometabolite accumulation (e.g. thailandamide & pyochelin) with exceptions (e.g. capistruin). However, we only quantified exometabolite accumulation in the shared medium reservoir. Differential release and uptake of bioactive molecules within the community can complicate tracking metabolite dynamics in the system. Thus, analyses that incorporate both intracellular and extracellular metabolomics can provide a more complete understanding of altered microbial metabolism under different conditions. Regardless, we documented non-additive accumulation of secondary metabolites involved in both competition strategies. This finding may have implications for high-order interactions, meaning, the nature of the interaction between two members may be altered by the addition of a third member (Billick and Case, 1994). For example, one member could produce sublethal antibiotics in the presence of an antibiotic-sensitive member. The addition of a third member could stimulate the antibiotic producer to increase antibiotic production, altering the nature of the initial interaction from sublethal to lethal for antibiotic-sensitive member (Bernier et al., 2013). In other words, the nature of interactions may be altered depending on

566 surrounding stimuli that can exacerbate bacterial behaviors not expected by studying
567 the system as simpler parts (Mickalide et al., 2019). Therefore, characterizing
568 transcriptome and metabolome dynamics in microbial communities is expected to
569 inform how non-additive phenomena arise and how they contribute to deviations in
570 predictive models of community outcomes.

571 Our results indicated that each member continued to maintain competitive
572 strategies despite stagnant population growth. In particular, *B. thailandensis*
573 upregulated various bioactive exometabolites involved in both interference and
574 exploitative competition when with neighbors. An effective competitor is often defined as
575 by its ability to outcompete neighbors via growth advantage that stems from efficient
576 nutrient uptake and/or biomass conversion rates (Miller et al., 2005; De Jong et al.,
577 2017). We add to this that a competitor can also have a fitness advantage through
578 effective maintenance, which can similarly employ interference or exploitative
579 competitive strategies despite no net growth. Maintenance may ensure survival in some
580 environments that impose a stationary phase lifestyle, where long periods of nutrient
581 depletion are punctuated with short periods of nutrient flux. In these scenarios, it
582 warrants to understand how competitive strategies are deployed in the interim of growth
583 and the extent to which these interactions contribute to long-term community outcomes.
584 Though population levels remain constant, sub-populations of growing cells have been
585 observed in stationary phase (Jõers et al., 2020), and continued production of
586 competitive exometabolites may serve as an advantageous strategy to hinder growth of
587 competitors. In addition, some antibiotics remain effective in non-replicating bacteria
588 (McCall et al., 2019). The ability for continued maintenance via effective competition

589 strategies during stationary phase may provide spatiotemporal maintenance of
590 population levels before growth resumption (Chesson, 1983). Thus, we expect that
591 insights into the long-term consequences of competition for microbial community
592 outcomes will be gained by considering competition in both active growth and
593 maintenance scenarios.

594

595 Material and Methods

596 **Bacterial strains and culture conditions**

597

598 Freezer stocks of *B. thailandensis*, *C. violaceum*, and *P. syringae* were plated on
599 half-concentration Trypticase soy agar (TSA50) at 27°C for at least 24 h. Strains were
600 inoculated in 7 ml of M9–0.2% glucose medium and grown for 16 h at 27°C, 200 rpm.
601 Cultures were then back-diluted into 50 ml M9-0.2% glucose medium such that
602 exponential growth phase was achieved after 10 h of incubation at 27°C, 200 rpm.
603 Strains were back-diluted in 50 ml M9 glucose medium to target ODs (*B. thailandensis*
604 0.3 OD, *C. violaceum*: 0.035 OD, *P. syringae* 0.035 OD) such that stationary phase
605 growth would be achieved by all members within a 2 h time frame after 24 h incubation
606 in the transwell plate. The glucose concentration in the final back-dilution varied upon
607 community arrangement- 0.067% for monocultures, 0.13% for pairwise cocultures, and
608 0.2% for the 3-member community. For each strain, 48 ml of back-diluted culture was
609 transferred as 4 mL aliquots in 12, 5 mL Falcon tubes prior to transferring them into the
610 transwell plate.

611

612 **Synthetic community experiments**

613

614 Transwell plate preparation was performed as previously described (Chodkowski
615 and Shade, 2017). Briefly, we used sterile filter plates with 0.22-µm-pore polyvinylidene
616 difluoride (PVDF) filter bottoms (Millipore MAGVS2210). Prior to use, filter plates were
617 washed three times with sterile water using a vacuum apparatus (NucleoVac 96
618 vacuum manifold; Clontech Laboratories). The filter of well H12 was removed with a
619 sterile pipette tip and tweezer, and 31 ml of M9 glucose medium was added to the
620 reservoir through well H12. The glucose concentration in the reservoir varied upon
621 community arrangement- 0.067% for monocultures, 0.13% for pairwise cocultures, and
622 0.2% for the 3-member community. Each well was then filled with 130 µL of culture or
623 medium. For each plate, a custom R script (RandomArray.R [see script at
624 https://github.com/ShadeLab/PAPER_Chodkowski_mSystems_2017/blob/master/R_an
625 alysis/RandomArray.R]) was used to randomize community member placement in the
626 wells so that each member occupied a total of 31 wells per plate. In total, there were 7
627 community conditions- 3 monocultures, 3 pairwise cocultures, and the 3-member
628 community. A time course was performed for each replicate. The time course included
629 an exponential phase time point (12.5 h) and 5 time points assessed every 5 h over
630 stationary phase (25 h – 45 h). Four biological replicates were performed for each
631 community condition for a total of 28 experiments. For each experiment, 6 replicate filter
632 plates were prepared for destructive sampling for a total of 168 transwell plates.

633

634 Filter plates were incubated at 27°C with gentle shaking (~0.32 rcf). For each
635 plate, a custom R script (RandomArray.R [see script at
636 https://github.com/ShadeLab/PAPER_Chodkowski_mSystems_2017/blob/master/R_an
637 alysis/RandomArray.R]) was used to randomize wells for each organism assigned to
638 RNA extraction (16 wells) and flow cytometry (5 wells). The following procedure was
639 performed for each organism when a transwell plate was destructively sampled: i) wells
640 containing spent culture assigned to RNA extraction were pooled into a 1.5 mL
641 microcentrifuge tube and flash frozen in liquid nitrogen and stored at -80 until further
642 processing. ii) 20 µL from wells assigned for flow cytometry were diluted into 180 µL
643 Tris-buffered saline (TBS; 20 mM Tris, 0.8% NaCl [pH 7.4]). In plate arrangements
644 where *P. syringae* was arrayed with *B. thailandensis*, *P. syringae* had a final dilution of
645 70-fold in TBS. In plate arrangements where *P. syringae* was arrayed in monoculture or
646 in coculture with *C. violaceum*, *P. syringae* had a final dilution of 900-fold in TBS. Final
647 dilutions for *B. thailandensis* and *C. violaceum* were 1,300-fold and 1,540-fold,
648 respectively. iii) Spent medium (~31 ml) from the shared reservoir was transferred to 50
649 mL conical tubes, flash-frozen in liquid nitrogen and stored at −80 °C prior to metabolite
650 extraction.
651
652 **Flow cytometry**
653
654 Diluted cultures were stained with the Thermo Scientific LIVE/DEAD BacLight
655 bacterial viability kit at final concentrations of 1.5 µM Syto9 (live stain) and 2.5 µM
656 propidium iodide (dead stain). Two hundred microliters of stained cultures were

657 transferred to a 96-well microtiter U-bottom microplate (Thermo Scientific). Twenty
658 microliters of sample were analyzed on a BD Accuri C6 flow cytometer (BD
659 Biosciences) at a fluidics rate of 66 µl/min and a threshold of 500 on an FL2 gate. The
660 instrument contained the following optical filters: FL1-533, 30 nm; FL2-585, 40 nm; and
661 FL3, 670-nm longpass. Data were analyzed using BD Accuri C6 software version
662 1.0.264.21 (BD Biosciences).
663
664 **RNA-seq**
665 *RNA extraction*
666 RNA was extracted using the E.Z.N.A. Bacterial RNA kit (Omega Bio-tek, Inc.). An in-
667 tube DNase I (Ambion, Inc AM2222, 2U) digestion was performed to remove DNA from RNA
668 samples. RNA samples were purified and concentrated using the Qiagen RNAeasy MinElute
669 Clean up Kit (Qiagen, Inc). Ten random samples were chosen to assess RNA integrity on an
670 Agilent 2100 Bioanalyzer.
671
672 *RNA sample prep, sequencing, QC, read preprocessing, and filtering*
673 Standard operating protocols were performed at the Department of Energy Joint
674 Genome Institute as previously described (Chodkowski and Shade, 2020).
675
676 *Pseudoalignment and counting*
677 Reads from each library with pseudoaligned to the transcriptome of each strain
678 with kallisto (Bray et al., 2016). Raw counts from each library were combined into a
679 gene count matrix for each strain. The gene count matrix was used for downstream
680 analyses.

681

682 **Transcriptomics**

683 *Quality filtering and differential gene expression analysis*

684 Count matrices for each member were quality filtered in two steps: genes
685 containing 0 counts in all samples were removed, and genes with a transcript count of
686 ≤10 in more than 90% of samples were removed. DESeq2 (Love et al., 2014) was used to
687 extract size factor and dispersion estimates. These estimates were used as external
688 input into ImpulseDE2 for the analysis of differentially regulated genes (Fischer et al.,
689 2018). Case-control (Cocultures-monoculture control) analyses were analyzed to
690 identify both permanent and transient regulated genes at an FDR-corrected threshold of
691 0.01. For each member, differences in gene regulation between the three coculture
692 conditions was visualized with venn diagrams using the VennDiagram package.
693 The initial differential gene expression analysis compared each coculture to the
694 monoculture control, separately. It was revealed that were was a subset of genes that
695 were only differentially expressed in the 3-member community. These genes were
696 parsed from the dataset and used to perform two additional analyses in ImpulseDE2.
697 Case-control analyses were performed to analyze differential expression between the 3-
698 member community to each of the pairwise cocultures as controls. Functional
699 enrichment analysis was performed on the collection of genes determined to have
700 unique differential expression in the 3-member community using the BiNGO package in
701 Cytoscape (Maere et al., 2005).

702

703 *COG analysis*

704 Protein fasta files were downloaded from NCBI and uploaded to eggNOG-
705 mapper v2 (http://eggnog-mapper.embl.de/) to obtain Clusters of Orthologous Groups
706 (COG) categories. Genes corresponding to COGs were categorized as upregulated or
707 downregulated based on their temporal expression patterns and plotted using ggplot2.
708
709 *Principal coordinates analysis and statistics*
710 We extracted genes that were differentially expressed with an FDR-corrected
711 threshold of < 0.01 and a log2 fold-change >1 or < -1. A variance-stabilizing
712 transformation was performed on normalized gene matrices using the rlog function in
713 DESeq2. A distance matrix based on the Bray-Curtis dissimilarity metric was then
714 calculated on the variance-stabilized gene matrices and principal coordinates analysis
715 was performed using the R package vegan. Principal coordinates were plotted using
716 ggplot2. Coordinates of the first two PCoA axes were used to perform Protest analysis
717 using the protest function in vegan. Dissimilarity matrices were used to perform
718 PERMANOVA and variation partitioning and using the adonis and varpart functions in
719 vegan, respectively. The RVAideMemoire package was used to perform a post-hoc
720 pairwise PERMANOVAs.
721
722 *Circos plots*
723 A subset of the top ~500 of differentially regulated genes was determined for
724 each member by assessing differential expression in the 3-member community. A log2
725 fold-change (LFC) cutoff of at least > 1.5 or < -1.5 was used to capture both upregulated
726 and downregulated genes. The LFC threshold needed to be met in at least one

727 timepoint. We then filtered these genes by those that had differential expression with a
728 significance cutoff of < 0.01 (FDR corrected). *P. syringae* genes encoded on plasmids
729 were an exception. We extracted all coding sequence genes from both plasmids
730 because the entirety of each plasmid could be visualized on a Circos plot with high
731 resolution. From these genes of interest, a variance-stabilizing transformation was
732 performed on normalized gene matrices using the rlog function in DESeq2 and Z-scored
733 on a per gene basis. Circular genome plots were generated in Circos version 0.69-5.
734 Pseudo-genes composed of the minimum and maximum Z-scores were added to each
735 of four tracks to make the Z-score color scale comparable across all community
736 arrangements. Functional enrichment analysis was performed on the collection of genes
737 within each *P. syringae* plasmid using the BiNGO package in Cytoscape.
738
739 *Biosynthetic gene cluster (BSGC) analysis*
740 NCBI accession numbers were uploaded to antiSMASH 6 beta bacterial version
741 (Blin et al., 2021) to identify genes involved in BSGCs using default parameters. Where
742 possible, literature-based evidence and BSGCs uploaded to MIBiG (Kautsar et al.,
743 2020) were used to better inform antiSMASH predictions. Log2 fold-changes (LFCs)
744 were calculated for all predicted biosynthetic genes within each predicted cluster by
745 comparing coculture expression to monoculture expression at each time point. Average
746 LFCs were calculated from all predicted biosynthetic genes within a predicted BSGC at
747 each time point. Temporal LFC trends were plotted using ggplot2. An upregulated
748 BSGC was defined as a BSGC that had at least two consecutive time points in
749 stationary phase with a LFC > 1.

750

751 *Network analysis*

752 Unweighted co-expression networks were created from quality filtered and
753 normalized expression data. Networks were generated for pairwise cocultures
754 containing *B. thailandensis*. First, data were quality filtered as previously described
755 (See section: *Quality filtering and differential gene expression analysis*). Then,
756 normalized expression data was extracted from DESeq2. Biological replicates for
757 each member within each timepoint were averaged by mean. Interspecies networks
758 were then inferred from the expression data using the context likelihood of relatedness
759 (Faith et al., 2007) algorithm within the R package Minet (Meyer et al., 2008). Gene
760 matrices for each coculture pair were concatenated to perform the following analysis.
761 Briefly, the mutual information coefficient was determined for each gene-pair. To ensure
762 robust detection of co-expressed genes, a resampling approach was used as previously
763 described (McClure et al., 2016). Then, a Z-score was computed on the mutual
764 information matrix. A Z-score threshold of 4.5 was used to determine an edge in the
765 interspecies network. Interspecies networks were uploaded into Cytoscape version
766 3.7.1. for visualization, topological analysis, and enrichment analysis (Shannon et al.,
767 2003).

768

769 Gene annotation and gene ontology files were obtained for *B. thailandensis*, *P.*
770 *syringae,* and *C. violaceum* for enrichment analyses. For *B. thailandensis,* annotation
771 and ontology files were downloaded from the Burkholderia Genome Database
772 (https://www.burkholderia.com). For *P. syringae*, annotation and ontology files were

773 downloaded from the Pseudomonas Genome Database
774 (http://www.pseudomonas.com/strain/download). Annotation and ontology files for *C.*
775 *violaceum* were generated using Blast2GO version 5.2.5 (Götz et al., 2008).
776 InterProScan (Zbobnov and Apweiler, 2001) with default parameters were used to
777 complement gene annotations from *C. violaceum*. GO terms were assigned using
778 Blast2GO with default parameters. In addition, genes involved in secondary metabolism
779 were manually curated and added to these files as individual GO terms. These genes
780 were also used to update the GO term GO**:**0017000 (antibiotic biosynthetic process),
781 composed of a collection of all the biosynthetic genes. (See section: *Biosynthetic gene*
782 *cluster analysis*).
783 Topological analysis was performed as follows: Nodes were filtered from each
784 coculture network to only select genes from one member. The GLay community cluster
785 function in Cytoscape was used to determine intra-member modules. Functional
786 enrichment analysis was then performed on the modules using the BiNGO package in
787 Cytoscape.
788
789 To determine interspecies co-regulation patterns, we filtered network nodes that
790 contained an interspecies edge. Functional enrichment analysis was performed on the
791 collection of genes containing interspecies edges for each member using the BiNGO
792 package in Cytoscape. Modules of interest (e.g. thailandamide and malleilactone) were
793 filtered in Cytoscape for visualization. The biosynthetic gene cluster organization of
794 thailandamide and malleilactone were obtained from MIbig and drawn in InkScape.
795

796 Protein sequences from an interspecies gene of interest from the thailandamide
797 module cluster (CLV_2968) and an interspecies gene of interest from the malleilactone
798 module cluster (PSPTO_1206) were obtained. A protein blast for each protein was run
799 against *B. thailandensis* protein sequences. *B. thailandensis* locus tags were extracted
800 from the top blast hit from each run. Normalized transcript counts for these 4 genes of
801 interest were plotted in R. Time course gene trajectories were determined using a loess
802 smoothing function.
803
804 *Non-additive gene expression*
805 The quality filtered and normalized expression matrix from each community
806 member was used to extract log2 fold-change (LFC) values within DESeq2. LFCs were
807 calculated by comparing transcript counts from each time point to its respective time
808 point in the monoculture condition. LFCs were converted to fold-changes (FC). Non-
809 additive outcomes were determined based on the null expectation that FCs in the 3-
810 member community should reflect a summation of FCs from the pairwise cocultures.
811 The thresholds for assigning a gene as non-additive upregulation was as follows:
812
813 (TM/MC)/(PWC1/MC+PWC2/MC) >1.2
814
815 Where TM are the gene counts in the 3-member community, MC are the gene counts in
816 the monoculture condition, and PWC1/PWC2 are the gene counts in the pairwise
817 coculture conditions 1 & 2, respectively. Non-additive gene expression patterns were
818 determined at each time point and plotted using ggplot2. Venn diagrams were also

819 created to analyze the patterns of non-additivity across the time series and between the
820 exponential phase time point and stationary phase times points. Functional enrichment
821 analysis was performed on the collection of genes determined to have non-additive
822 upregulation using the BiNGO package in Cytoscape.
823
824 **Metabolomics**
825
826 *LCMS sample preparation* and *data acquisition*
827 Standard operating protocols were performed at the Department of Energy Joint
828 Genome Institute as previously described (Chodkowski and Shade, 2020).
829
830 *Feature detection*
831 MZmine2 (Pluskal et al., 2010) was used for feature detection and peak area
832 integration as previously described (Chodkowski and Shade, 2017). Select
833 exometabolites were identified in MZmine2 by manual observation of both MS and
834 MS/MS data. We extracted quantities of these identified exometabolites for ANOVA and
835 Tukey HSD post-hoc analysis in R.
836
837 *Feature filtering and HM visualization*
838 We filtered features in three steps to identify coculture-accumulated
839 exometabolites. The feature-filtering steps were performed as follows on a per-member
840 basis: (i) retain features where the maximum peak area abundance occurred in a
841 coculture community arrangement ; (ii) a noise filter, the minimum peak area of a

842 feature from a replicate at any time point needed to be 3 times the maximum peak area
843 of the same feature in one of the external control replicates, was applied; (iii) coefficient
844 of variation (CV) values for each feature calculated between replicates at each time
845 point needed to be less than 20% across the time series.
846 Four final feature data sets from polar and nonpolar analyses in both ionization modes
847 were analyzed in MetaboAnalyst 5.0 (Pang et al., 2021). Features were normalized by
848 an ITSD reference feature (see Dataset 5
849 at https://github.com/ShadeLab/Paper_Chodkowski_MonocultureExometabolites_2020/t
850 ree/master/Datasets) and cube root transformed. Reference features for polar analyses
851 in positive ([^{13}C,^{15}N]proline) and negative ([^{13}C,^{15}N]alanine) modes were determined by
852 the ITSD with the lowest CV value across all samples. The reference feature for
853 nonpolar data sets was the ITSD ABMBA. Heat maps were generated in MetaboAnalyst
854 using Ward's clustering algorithm with Euclidean distances from Z-scored data. Data for
855 each sample are the averages from independent time point replicates (n = 2 to 4).
856 Normalized and transformed data sets were exported from MetaboAnalyst to generate
857 principal-coordinate analysis (PCoA) plots in R.
858
859 *Principal coordinates analysis and statistics*
860 A distance matrix based on the Bray-Curtis dissimilarity metric was used to
861 calculate dissimilarities between exometabolite profiles. Principal coordinates analysis
862 was performed using the R package vegan. Principal coordinates were plotted using
863 ggplot2. Coordinates of the first two PCoA axes were used to perform Protest analysis
864 using the protest function in vegan. Dissimilarity matrices were used to perform

865 PERMANOVA and variation partitioning and using the adonis and varpart functions in
866 vegan, respectively. The RVAideMemoire package was used to perform a post-hoc
867 pairwise PERMANOVAs. Monoculture community arrangements were removed to focus
868 on coculture trends.
869
870 *Non-additive metabolomics production*
871 All reference standard normalized, filtered features (across both polarities and
872 ionization modes) were combined. Non-additive outcomes were determined based on
873 the null expectation that fold-changes (FC) in the 3-member community should reflect a
874 summation of FCs from the pairwise cocultures. The thresholds for assigning a
875 metabolomic feature as non-additive production was as follows:
876
877 $(TM)/(PWC1 + PWC2 + PWC3) > 1.5$
878
879 Where TM is the peak area abundance in the 3-member community, and
880 PWC1/PWC2/PWC2 are the peak area abundance in the pairwise coculture conditions
881 1,2, and 3, respectively. FCs were determined at each time point. A feature was
882 determined to be produced in the 3-member community in a non-additive manner if it
883 was above the FC threshold at least 3 times during stationary phase. At each time point,
884 a Z-scored distribution of FCs was plotted in R. Z-scores were extracted from
885 exometabolite of interest (thailandamide, pyochelin, and capistruin) to plot as vertical
886 ablines on the Z-scored distributions. In addition, the non-additive features were
887 extracted from the dataset to generate a heat map in MetaboAnalyst. Ward's clustering

algorithm was used with Euclidean distances from Z-scored data. Data for each sample are the averages from independent time point replicates (n = 2 to 4).

To find statistical support for non-additive exometabolite production in the 3-member community, we created an “expected” time course abundance for identified exometabolites that had non-additive upregulation (thailandamide, pyochelin, and capistruin). The “expected” time course abundance was determined by calculating the summation of peak abundances across pairwise cocultures with *B. thailandensis*. Due to the issue of replicate independence for each time course, the standard deviation would vary depending on what replicates were combined. As a conservative approach, we permuted all possible pairwise coculture combinations and used the replicate combination that resulted in the highest standard deviation. The time course peak abundance of thailandamide, pyochelin, and capistruin from pairwise cocultures with *B. thailandensis*, from the 3-member community, and from the “expected” 3-member community were plotted in ggplot2. We then ran a repeated measures permutation ANOVA to compare the time course peak abundance of thailandamide, pyochelin, and capistruin observed in the 3-member community to the “expected” 3-member community. A post-hoc pairwise t-test was performed to observe which time points were statistically significant. We note each iteration of repeated measures ANOVA would result in different statistical result. This was because the replicate identifiers for the “expected” time course were arbitrarily assigned. For this reason, we only considered a test significant if it was consistently below a P threshold of 0.05 across 10 iterations of the code.

911

912 **Code availability**

913 Computing code, workflows, and data sets are available at
914 [https://github.com/ShadeLab/Paper_Chodkowski_3member_SynCom_2021]. R
915 packages used during computing analyses included DEseq2 (Love et al., 2014),
916 ImpulseDE2 (Fischer et al., 2018), Minet (Meyer et al., 2008), vegan 2.5-4 (Oksanen et
917 al., 2019), ggplot2 (Wickham, 2016), VennDiagram (Chen, 2018), RVAideMemoire
918 (Herve, 2020), rtracklayer (Lawrence et al., 2009), viridis (Garnier et al., 2021), and
919 helper functions (Wickham, 2007, Wickham, 2019; Wickham et al., 2019A; Wickham et
920 al., 2019B).

921

922 **Data availability**

923 Genomes for *B. thailandensis*, *C. violaceum*, and *P. syringae* are available at the
924 National Center for Biotechnology Information (NCBI) under accession
925 numbers NC_007651 (Chromosome I)/NC_007650 (Chromosome
926 II), NZ_PKBZ01000001, and NC_004578 (Chromosome)/NC_004633 (Plasmid
927 A)/NC_004632 (Plasmid B), respectively. An improved annotated draft genome of *C.*
928 *violaceum* is available under NCBI BioProject accession
929 number PRJNA402426 (GenBank accession number PKBZ00000000). Data for
930 resequencing efforts for *B. thailandensis* and *P. syringae* are under NCBI BioProject
931 accession numbers PRJNA402425 and PRJNA402424, respectively. Metabolomics
932 data and transcriptomics data are also available at the JGI Genome Portal (Nordberg et
933 al., 2014) under JGI proposal identifier 502921. MZmine XML parameter files for all

934 analyses can be viewed at and downloaded from GitHub (see Dataset 7
935 at https://github.com/ShadeLab/Paper_Chodkowski_MonocultureExometabolites_2020/t
936 ree/master/Datasets). Large data files (e.g., MZmine project files) are available upon
937 request. Supplementary files are also available on GitHub
938 (https://github.com/ShadeLab/Paper_Chodkowski_3member_SynCom_2021/tree/maste
939 r/Supplemental_Files).
940

941 **Acknowledgements**

942 This material is based upon work supported by the National Science Foundation under
943 grant DEB 1749544 and by Michigan State University. In addition, metabolite analysis
944 and transcript sequencing were provided by a DOE-JGI Community Science Program
945 award (proposal identifier 502921). The work conducted by the U.S. Department of
946 Energy Joint Genome Institute, a DOE Office of Science User Facility, is supported
947 under contract number DE-AC02-05CH11231. J.L.C. was supported by the Eleanor L.
948 Gilmore Fellowship from the Department of Microbiology and Molecular Genetics.

949 We thank Katherine B. Louie and Benjamin P. Bowen for support in mass spectral
950 analysis.
951

952 **Competing Interests**

953 We declare no competing interests.
954

Author contributions

J.L.C. and A.S. conceived of and designed the study. J.L.C. performed the research and analyses. J.L.C. and A.S. wrote the manuscript.

References

Alice, A. F., López, C. S., Lowe, C. A., Ledesma, M. A., & Crosa, J. H. (2006). Genetic and transcriptional analysis of the siderophore malleobactin biosynthesis and transport genes in the human pathogen Burkholderia pseudomallei K96243. *Journal of Bacteriology*, *188*(4), 1551–1566. https://doi.org/10.1128/JB.188.4.1551-1566.2006

Amunts, A., Fiedorczuk, K., Truong, T. T., Chandler, J., Peter Greenberg, E., & Ramakrishnan, V. (2015). Bactobolin A binds to a site on the 70S ribosome distinct from previously seen antibiotics. *Journal of Molecular Biology*, *427*(4), 753–755. https://doi.org/10.1016/j.jmb.2014.12.018

Antwis, R. E., Griffiths, S. M., Harrison, X. A., Aranega-Bou, P., Arce, A., Bettridge, A. S., … Sutherland, W. J. (2017). Fifty important research questions in microbial ecology. *FEMS Microbiology Ecology*, *93*(5), fix044. https://doi.org/10.1093/femsec/fix044

Aziz, F. A. A., Suzuki, K., Ohtaki, A., Sagegami, K., Hirai, H., Seno, J., … Futamata, H. (2015). Interspecies interactions are an integral determinant of microbial community dynamics. *Frontiers in Microbiology*, *6*, 1148. https://doi.org/10.3389/fmicb.2015.01148

Bernier, S. P., & Surette, M. G. (2013). Concentration-dependent activity of antibiotics in natural environments. Frontiers in Microbiology, 4, 20. https://doi.org/10.3389/fmicb.2013.00020

Biggins, J. B., Ternei, M. A., & Brady, S. F. (2012). Malleilactone, a polyketide synthase-derived virulence factor encoded by the cryptic secondary metabolome of Burkholderia pseudomallei group pathogens. *Journal of the American Chemical Society*, *134*(32), 13192–13195. https://doi.org/10.1021/ja3052156

Billick, I., & Case, T. J. (1994). Higher order interactions in ecological communities: What are they and how can they be detected? *Ecology*, *75*(6), 1529–1543. https://doi.org/10.2307/1939614

Blin, K., Shaw, S., Kloosterman, A. M., Charlop-Powers, Z., van Wezel, G. P., Medema, M. H., & Weber, T. (2021). antiSMASH 6.0: improving cluster detection and comparison capabilities. Nucleic Acids Research, 49(W1), W29–W35. https://doi.org/10.1093/NAR/GKAB335

Bray, N. L., Pimentel, H., Melsted, P., & Pachter, L. (2016). Near-optimal probabilistic RNA-seq quantification. *Nature Biotechnology*, *34*, 525–527. https://doi.org/10.1038/nbt.3519

Brett, P. J., DeShazer, D., & Woods, D. E. (1998). Burkholderia thailandensis sp. nov., a Burkholderia pseudomallei-like species. International Journal of Systematic Bacteriology, 48 Pt 1(1), 317–320. https://doi.org/10.1099/00207713-48-1-317

Browning, D. F., & Busby, S. J. W. (2004). The regulation of bacterial transcription initiation. *Nature Reviews Microbiology*, *2*(1), 57–65. https://doi.org/10.1038/nrmicro787

Buell, C. R., Joardar, V., Lindeberg, M., Selengut, J., Paulsen, I. T., Gwinn, M. L., … Collmer, A. (2003). The complete genome sequence of the Arabidopsis and tomato pathogen Pseudomonas syringae pv. tomato DC3000. Proceedings of the National Academy of Sciences, 100(18), 10181–10186. https://doi.org/10.1073/PNAS.1731982100

Bundy, B. M., Collier, L. S., Hoover, T. R., & Neidle, E. L. (2002). Synergistic transcriptional activation by one regulatory protein in response to two metabolites. *Proceedings of the National Academy of Sciences of the United States of America*, *99*(11), 7693–7698. https://doi.org/10.1073/pnas.102605799

Butt, A. T., & Thomas, M. S. (2017). Iron acquisition mechanisms and their role in the virulence of Burkholderia species. *Frontiers in Cellular and Infection Microbiology*, *7*, 460. https://doi.org/10.3389/fcimb.2017.00460

Chandler, J. R., Heilmann, S., Mittler, J. E., & Greenberg, E. P. (2012). Acyl-homoserine lactone-dependent eavesdropping promotes competition in a laboratory co-culture model. *ISME Journal*, *6*(12), 2219–2228. https://doi.org/10.1038/ismej.2012.69

Chen, H. (2018). VennDiagram: Generate High-Resolution Venn and Euler Plots. R package version 1.6.20.

Chesson, P. L. (1983). Coexistence of Competitors in a Stochastic Environment: The Storage Effect. *Lecture Notes in Biomathematics*, *52*, 188–198. https://doi.org/10.1007/978-3-642-87893-0_25

Chiesa, S. C., Irvine, R. L., & Manning, J. F. (1985). Feast/famine growth environments and activated sludge population selection. *Biotechnology and Bioengineering*, *27*(5), 562–568. https://doi.org/10.1002/bit.260270503

Chodkowski, J. L., & Shade, A. (2020). Exometabolite Dynamics over Stationary Phase Reveal Strain-Specific Responses. *MSystems*, *5*(6), e00493-20. https://doi.org/10.1128/msystems.00493-20

Chodkowski, J. L., & Shade, A. (2017). A Synthetic Community System for Probing Microbial Interactions Driven by Exometabolites. *MSystems*, *2*(6), e00129-17. https://doi.org/10.1128/msystems.00129-17

Čihák, M., Kameník, Z., Šmídová, K., Bergman, N., Benada, O., Kofronová, O., … Bobek, J. (2017). Secondary metabolites produced during the germination of Streptomyces coelicolor. *Frontiers in Microbiology*, *8*, 2495. https://doi.org/10.3389/fmicb.2017.02495

Cornforth, D. M., & Foster, K. R. (2013). Competition sensing: The social side of bacterial stress responses. *Nature Reviews Microbiology*, *11*(4), 285–293. https://doi.org/10.1038/nrmicro2977

Cornforth, D. M., Popat, R., McNally, L., Gurney, J., Scott-Phillips, T. C., Ivens, A., … Brown, S. P. (2014). Combinatorial quorum sensing allows bacteria to resolve their social and physical environment. *Proceedings of the National Academy of Sciences of the United States of America*, *111*(11), 4280–4284. https://doi.org/10.1073/pnas.1319175111

Coyte, K. Z., Schluter, J., & Foster, K. R. (2015). The ecology of the microbiome: Networks, competition, and stability. *Science*, *350*(6261), 663–666. https://doi.org/10.1126/science.aad2602

D'hoe, K., Vet, S., Faust, K., Moens, F., Falony, G., Gonze, D., … Raes, J. (2018). Integrated culturing, modeling and transcriptomics uncovers complex interactions and emergent behavior in a three-species synthetic gut community. *ELife*, *7*, e37090. https://doi.org/10.7554/eLife.37090

De Jong, H., Casagranda, S., Giordano, N., Cinquemani, E., Ropers, D., Geiselmann, J., & Gouzé, J. L. (2017). Mathematical modelling of microbes: Metabolism, gene expression and growth. *Journal of the Royal Society Interface*, *14*(136), 20170502. https://doi.org/10.1098/rsif.2017.0502

De Roy, K., Marzorati, M., Van den Abbeele, P., Van de Wiele, T., & Boon, N. (2014). Synthetic microbial ecosystems: an exciting tool to understand and apply microbial communities. *Environmental Microbiology*, *16*(6), 1472–1481. https://doi.org/10.1111/1462-2920.12343

Dubeau, D., Déziel, E., Woods, D. E., & Lépine, F. (2009). Burkholderia thailandensis harbors two identical rhl gene clusters responsible for the biosynthesis of rhamnolipids. *BMC Microbiology*, *9*(1), 1–12. https://doi.org/10.1186/1471-2180-9-263

Duerkop, B. A., Varga, J., Chandler, J. R., Peterson, S. B., Herman, J. P., Churchill, M. E. A., … Greenberg, E. P. (2009). Quorum-sensing control of antibiotic synthesis in Burkholderia thailandensis. *Journal of Bacteriology*, *191*(12), 3909–3918. https://doi.org/10.1128/JB.00200-09

Estrela, S., Sanchez-Gorostiaga, A., Vila, J. C. C., & Sanchez, A. (2021). Nutrient dominance governs the assembly of microbial communities in mixed nutrient environments. *ELife*, *10*, e65948. https://doi.org/10.7554/eLife.65948

Evans, K. C., Benomar, S., Camuy-Vélez, L. A., Nasseri, E. B., Wang, X., Neuenswander, B., & Chandler, J. R. (2018). Quorum-sensing control of antibiotic resistance stabilizes cooperation in Chromobacterium violaceum. *ISME J*, *12*(5), 1263–1272. https://doi.org/10.1038/s41396-018-0047-7

Faith, J. J., Hayete, B., Thaden, J. T., Mogno, I., Wierzbowski, J., Cottarel, G., … Gardner, T. S. (2007). Large-scale mapping and validation of Escherichia coli transcriptional regulation from a compendium of expression profiles. *PLoS Biology*, *5*(1), e8. https://doi.org/10.1371/journal.pbio.0050008

Fetissov, S. O. (2017). Role of the gut microbiota in host appetite control: Bacterial growth to animal feeding behaviour. *Nature Reviews Endocrinology*, *13*(1), 11–25. https://doi.org/10.1038/nrendo.2016.150

Fischer, D. S., Theis, F. J., & Yosef, N. (2018). Impulse model-based differential expression analysis of time course sequencing data. *Nucleic Acids Research*, *46*(20), 119. https://doi.org/10.1093/nar/gky675

Foster, K. R., & Bell, T. (2012). Competition, not cooperation, dominates interactions among culturable microbial species. *Current Biology*, *22*(19), 1845–1850. https://doi.org/10.1016/j.cub.2012.08.005

Garnier, S., Ross, N., Rudis, R., Camargo, P. A., Sciaini, M., & Scherer, C. (2021). viridis - Colorblind-Friendly Color Maps for R, *R package*, https://sjmgarnier.github.io/viridis/. https://doi.org/10.5281/zenodo.4679424

Garren, M., Son, K., Tout, J., Seymour, J. R., & Stocker, R. (2016). Temperature-induced behavioral switches in a bacterial coral pathogen. *ISME Journal*, *10*(6), 1363–1372. https://doi.org/10.1038/ismej.2015.216

Ghoul, M., & Mitri, S. (2016). The Ecology and Evolution of Microbial Competition. *Trends in Microbiology*, *24*(10), 833–845. https://doi.org/10.1016/j.tim.2016.06.011

Goh, E. B., Yim, G., Tsui, W., McClure, J. A., Surette, M. G., & Davies, J. (2002). Transcriptional modulation of bacterial gene expression by subinhibitory concentrations of antibiotics. *Proceedings of the National Academy of Sciences of the United States of America*, *99*(26), 17025–17030. https://doi.org/10.1073/pnas.252607699

Götz, S., García-Gómez, J. M., Terol, J., Williams, T. D., Nagaraj, S. H., Nueda, M. J., … Conesa, A. (2008). High-throughput functional annotation and data mining with the Blast2GO suite. *Nucleic Acids Research*, *36*(10), 3420–3435. https://doi.org/10.1093/nar/gkn176

Großkopf, T., & Soyer, O. S. (2014). Synthetic microbial communities. *Current Opinion in Microbiology*, *18*(1), 72–77. https://doi.org/10.1016/j.mib.2014.02.002

Gupta, A., Bedre, R., Thapa, S. S., Sabrin, A., Wang, G., Dassanayake, M., & Grove, A. (2017). Global Awakening of Cryptic Biosynthetic Gene Clusters in Burkholderia thailandensis. *ACS Chemical Biology*, *12*(12), 3012–3021. https://doi.org/10.1021/acschembio.7b00681

Herve M. (2020). RVAideMemoire: testing and plotting procedures for biostatistics. R Packag version 09-77.

Hibbing, M. E., Fuqua, C., Parsek, M. R., & Peterson, S. B. (2010). Bacterial competition: Surviving and thriving in the microbial jungle. *Nature Reviews Microbiology*, *8*(1), 15–25. https://doi.org/10.1038/nrmicro2259

Hiltunen, T., Laakso, J., Kaitala, V., Suomalainen, L. R., & Pekkonen, M. (2008). Temporal variability in detritus resource maintains diversity of bacterial communities. *Acta Oecologica*, *33*(3), 291–299. https://doi.org/10.1016/j.actao.2007.12.002

Holt, R. D. (2008). Theoretical perspectives on resource pulses. *Ecology*, *89*(3), 671–681. https://doi.org/10.1890/07-0348.1

Ishida, K., Lincke, T., Behnken, S., & Hertweck, C. (2010). Induced biosynthesis of cryptic polyketide metabolites in a Burkholderia thailandensis quorum sensing mutant. *Journal of the American Chemical Society*, *132*(40), 13966–13968. https://doi.org/10.1021/ja105003g

Jõers, A., Liske, E., & Tenson, T. (2020). Dividing subpopulation of Escherichia coli in stationary phase. *Research in Microbiology*, *171*(3–4), 153–157. https://doi.org/10.1016/j.resmic.2020.02.002

Karas, V. O., Westerlaken, I., & Meyer, A. S. (2015). The DNA-binding protein from starved cells (Dps) utilizes dual functions to defend cells against multiple stresses. *Journal of Bacteriology*, *197*(19), 3206–3215. https://doi.org/10.1128/JB.00475-15

Kato, S., Haruta, S., Cui, Z. J., Ishii, M., & Igarashi, Y. (2005). Stable coexistence of five bacterial strains as a cellulose-degrading community. *Applied and Environmental Microbiology*, *71*(11), 7099–7106. https://doi.org/10.1128/AEM.71.11.7099-7106.2005

Kautsar, S. A., Blin, K., Shaw, S., Navarro-Muñoz, J. C., Terlouw, B. R., van der Hooft, J. J. J., … Medema, M. H. (2020). MIBiG 2.0: a repository for biosynthetic gene clusters of known function. Nucleic Acids Research, 48(D1), D454–D458. https://doi.org/10.1093/NAR/GKZ882

Kell, D. B., Brown, M., Davey, H. M., Dunn, W. B., Spasic, I., & Oliver, S. G. (2005). Metabolic footprinting and systems biology: The medium is the message. *Nature Reviews Microbiology*, *3*(7), 557–565. https://doi.org/10.1038/nrmicro1177

Knappe, T. A., Linne, U., Zirah, S., Rebuffat, S., Xie, X., & Marahiel, M. A. (2008). Isolation and structural characterization of capistruin, a lasso peptide predicted from the genome sequence of Burkholderia thailandensis E264. *Journal of the American Chemical Society*, *130*(34), 11446–11454. https://doi.org/10.1021/ja802966g

Konopka, A. (2009). What is microbial community ecology. *ISME J*, *3*(11), 1223–1230. https://doi.org/10.1038/ismej.2009.88

Kuznedelov, K., Semenova, E., Knappe, T. A., Mukhamedyarov, D., Srivastava, A., Chatterjee, S., … Severinov, K. (2011). The antibacterial threaded-lasso peptide capistruin inhibits bacterial RNA polymerase. *Journal of Molecular Biology*, *412*(5), 842–848. https://doi.org/10.1016/j.jmb.2011.02.060

Lawrence, M., Gentleman, R., & Carey, V. (2009). rtracklayer: An R package for interfacing with genome browsers. *Bioinformatics*, *25*(14), 1841–1842. https://doi.org/10.1093/bioinformatics/btp328

Li, A., Mao, D., Yoshimura, A., Rosen, P. C., Martin, W. L., Gallant, É., … Seyedsayamdost, M. R. (2020). Multi-omic analyses provide links between low-dose antibiotic treatment and induction of secondary metabolism in Burkholderia thailandensis. *MBio*, *11*(1), e03210-19. https://doi.org/10.1128/mBio.03210-19

Little, A. E. F., Robinson, C. J., Peterson, S. B., Raffa, K. F., & Handelsman, J. (2008). Rules of engagement: Interspecies interactions that regulate microbial communities. *Annual Review of Microbiology*, *62*, 375–401. https://doi.org/10.1146/annurev.micro.030608.101423

Love, M. I., Huber, W., & Anders, S. (2014). Moderated estimation of fold change and dispersion for RNA-seq data with DESeq2. *Genome Biology*, *15*, 550. https://doi.org/10.1186/s13059-014-0550-8

Maere, S., Heymans, K., & Kuiper, M. (2005). BiNGO: a Cytoscape plugin to assess overrepresentation of gene ontology categories in biological networks. Bioinformatics (Oxford, England), 21(16), 3448–3449. https://doi.org/10.1093/BIOINFORMATICS/BTI551

Mao, D., Bushin, L. B., Moon, K., Wu, Y., & Seyedsayamdost, M. R. (2017). Discovery of scmR as a global regulator of secondary metabolism and virulence in Burkholderia thailandensis E264. *Proceedings of the National Academy of Sciences of the United States of America*, *114*(14), E2920–E2928. https://doi.org/10.1073/pnas.1619529114

McCall, I. C., Shah, N., Govindan, A., Baquero, F., & Levin, B. R. (2019). Antibiotic killing of diversely generated populations of nonreplicating bacteria. *Antimicrobial Agents and Chemotherapy*, *63*(7), e02360-18. https://doi.org/10.1128/AAC.02360-18

McClure, R. S. (2019). Toward a Better Understanding of Species Interactions through Network Biology. *MSystems*, *4*(3), e00114-19. https://doi.org/10.1128/msystems.00114-19

McClure, R. S., Overall, C. C., Hill, E. A., Song, H.-S., Charania, M., Bernstein, H. C., … Beliaev, A. S. (2018). Species-specific transcriptomic network inference of interspecies interactions. *ISME J*, *12*(8), 2011–2023. https://doi.org/10.1038/s41396-018-0145-6

McClure, R. S., Overall, C. C., Mcdermott, J. E., Hill, E. A., Markillie, L. M., Mccue, L. A., … Beliaev, A. S. (2016). Network analysis of transcriptomics expands regulatory landscapes in Synechococcus sp. PCC 7002. *Nucleic Acids Research*, *44*(18), 8810–8825. https://doi.org/10.1093/nar/gkw737

Medema, M. H., Kottmann, R., Yilmaz, P., Cummings, M., Biggins, J. B., Blin, K., … Glöckner, F. O. (2015). Minimum Information about a Biosynthetic Gene cluster. *Nature Chemical Biology*, *11*(9), 625–631. https://doi.org/10.1038/nchembio.1890

Megan Steinweg, J., Dukes, J. S., Paul, E. A., & Wallenstein, M. D. (2013). Microbial responses to multi-factor climate change: Effects on soil enzymes. *Frontiers in Microbiology*, *4*, 146. https://doi.org/10.3389/fmicb.2013.00146

Meyer, P. E., Lafitte, F., & Bontempi, G. (2008). Minet: A r/bioconductor package for inferring large transcriptional networks using mutual information. *BMC Bioinformatics*, *9*(1), 461. https://doi.org/10.1186/1471-2105-9-461

Mickalide, H., & Kuehn, S. (2019). Higher-Order Interaction between Species Inhibits Bacterial Invasion of a Phototroph-Predator Microbial Community. *Cell Systems*, *9*(6), 521-533.e10. https://doi.org/10.1016/j.cels.2019.11.004

Miller, T. E., Burns, J. H., Munguia, P., Walters, E. L., Kneitel, J. M., Richards, P. M., … Buckley, H. L. (2005). A critical review of twenty years' use of the resource-ratio theory. *American Naturalist*, *165*(4), 439–448. https://doi.org/10.1086/428681

Momeni, B., Xie, L., & Shou, W. (2017). Lotka-Volterra pairwise modeling fails to capture diverse pairwise microbial interactions. *ELife*, *6*, e25051. https://doi.org/10.7554/eLife.25051.001

Morin, M., Pierce, E. C., & Dutton, R. J. (2018). Changes in the genetic requirements for microbial interactions with increasing community complexity. *ELife*, *7*, e37072. https://doi.org/10.7554/eLife.37072

Nair, S., & Finkel, S. E. (2004). Dps protects cells against multiple stresses during stationary phase. *Journal of Bacteriology*, *186*(13), 4192–4198. https://doi.org/10.1128/JB.186.13.4192-4198.2004

Navarro Llorens, J. M., Tormo, A., & Martínez-García, E. (2010). Stationary phase in gram-negative bacteria. *FEMS Microbiology Reviews*, *34*(4), 476–495. https://doi.org/10.1111/j.1574-6976.2010.00213.x

Netzker, T., Fischer, J., Weber, J., Mattern, D. J., König, C. C., Valiante, V., … Brakhage, A. A. (2015). Microbial communication leading to the activation of silent fungal secondary metabolite gene clusters. *Frontiers in Microbiology*. Frontiers Media S.A. https://doi.org/10.3389/fmicb.2015.00299

Nordberg, H., Cantor, M., Dusheyko, S., Hua, S., Poliakov, A., Shabalov, I., … Dubchak, I. (2014). The genome portal of the Department of Energy Joint Genome Institute: 2014 updates. *Nucleic Acids Research*, *42*, D26-31. https://doi.org/10.1093/nar/gkt1069

Okada, B. K., & Seyedsayamdost, M. R. (2017). Antibiotic dialogues: Induction of silent biosynthetic gene clusters by exogenous small molecules. *FEMS Microbiology Reviews*, *41*(1), 19–33. https://doi.org/10.1093/femsre/fuw035

Okada, B. K., Wu, Y., Mao, D., Bushin, L. B., & Seyedsayamdost, M. R. (2016). Mapping the Trimethoprim-Induced Secondary Metabolome of Burkholderia thailandensis. *ACS Chemical Biology*, *11*(8), 2124–2130. https://doi.org/10.1021/acschembio.6b00447

Oksanen, J., Blanchet, F. G., Friendly, M., Kindt, R., Legendre, P., McGlinn, D., … Wagner, H. (2019). vegan: Community Ecology Package. R package version 2.5-4.

Orr, J. A., Vinebrooke, R. D., Jackson, M. C., Kroeker, K. J., Kordas, R. L., Mantyka-Pringle, C., … Piggott, J. J. (2020). Towards a unified study of multiple stressors: Divisions and common goals across research disciplines. *Proceedings of the Royal Society B: Biological Sciences*, *287*(1926), 20200421. https://doi.org/10.1098/rspb.2020.0421

Ortiz, A., Vega, N. M., Ratzke, C., & Gore, J. (2021). Interspecies bacterial competition regulates community assembly in the C. elegans intestine. *ISME J*, 1–15. https://doi.org/10.1038/s41396-021-00910-4

Pacheco, A. R., Osborne, M. L., & Segrè, D. (2021). Non-additive microbial community responses to environmental complexity. *Nature Communications*, *12*(1), 1–11. https://doi.org/10.1038/s41467-021-22426-3

Pang, Z., Chong, J., Zhou, G., de Lima Morais, D. A., Chang, L., Barrette, M., … Xia, J. (2021). MetaboAnalyst 5.0: narrowing the gap between raw spectra and functional insights. *Nucleic Acids Research*, (1), gkab382. https://doi.org/10.1093/nar/gkab382

Pekkonen, M., Korhonen, J., & Laakso, J. T. (2011). Increased survival during famine improves fitness of bacteria in a pulsed-resource environment. *Evolutionary Ecology Research* (Vol. 13). Evolutionary Ecology, Ltd.

Pettit, R. K. (2009). Mixed fermentation for natural product drug discovery. *Applied Microbiology and Biotechnology*, *83*(1), 19–25. https://doi.org/10.1007/s00253-009-1916-9

Phelan, V. V, Liu, W.-T., Pogliano, K., & Dorrestein, P. C. (2011). Microbial metabolic exchange--the chemotype-to-phenotype link. *Nature Chemical Biology*, *8*(1), 26–35. https://doi.org/10.1038/nchembio.739

Pietschke, C., Treitz, C., Forêt, S., Schultze, A., Künzel, S., Tholey, A., … Fraune, S. (2017). Host modification of a bacterial quorum-sensing signal induces a phenotypic switch in bacterial symbionts. *Proceedings of the National Academy of Sciences of the United States of America*, *114*(40), E8488–E8497. https://doi.org/10.1073/pnas.1706879114

Pinu, F. R., & Villas-Boas, S. G. (2017). Extracellular microbial metabolomics: The state of the art. *Metabolites*, *7*(3), 43. https://doi.org/10.3390/metabo7030043

Pluskal, T., Castillo, S., Villar-Briones, A., & Orešič, M. (2010). MZmine 2: Modular framework for processing, visualizing, and analyzing mass spectrometry-based molecular profile data. *BMC Bioinformatics*, *11*, 395. https://doi.org/10.1186/1471-2105-11-395

Sanchez-Gorostiaga, A., Bajić, D., Osborne, M. L., Poyatos, J. F., & Sanchez, A. (2019). High-order interactions distort the functional landscape of microbial consortia. *PLoS Biology*, *17*(12), e3000550. https://doi.org/10.1371/journal.pbio.3000550

Schimel, J. P. (2018). Life in dry soils: Effects of drought on soil microbial communities and processes. *Annual Review of Ecology, Evolution, and Systematics*, *49*, 409–432. https://doi.org/10.1146/annurev-ecolsys-110617-062614

Shannon, P., Markiel, A., Ozier, O., Baliga, N. S., Wang, J. T., Ramage, D., … Ideker, T. (2003). Cytoscape: A software Environment for integrated models of biomolecular interaction networks. *Genome Research*, *13*(11), 2498–2504. https://doi.org/10.1101/gr.1239303

Silva, L. P., & Northen, T. R. (2015). Exometabolomics and MSI: Deconstructing how cells interact to transform their small molecule environment. *Current Opinion in Biotechnology*, *34*, 209–216. https://doi.org/10.1016/j.copbio.2015.03.015

Smith, H. L. (2011). Bacterial competition in serial transfer culture. *Mathematical Biosciences*, *229*(2), 149–159. https://doi.org/10.1016/j.mbs.2010.12.001

Stewart, F. M., & Levin, B. R. (1973). Partitioning of Resources and the Outcome of Interspecific Competition: A Model and Some General Considerations. *The American Naturalist*, *107*(954), 171–198. https://doi.org/10.1086/282825

Stock, A. M., Robinson, V. L., & Goudreau, P. N. (2000). Two-component signal transduction. *Annual Review of Biochemistry*. Annual Reviews 4139 El Camino Way, P.O. Box 10139, Palo Alto, CA 94303-0139, USA. https://doi.org/10.1146/annurev.biochem.69.1.183

Stock, A. M., Robinson, V. L., & Goudreau, P. N. (2000). Two-component signal transduction. *Annual Review of Biochemistry*, *69*, 183–215. https://doi.org/10.1146/annurev.biochem.69.1.183

Tilman, D. (1982). *Resource Competition and Community Structure*. Princeton, NJ, U.S.A.: Princeton University Press.

Truong, T. T., Seyedsayamdost, M., Greenberg, E. P., & Chandler, J. R. (2015). A Burkholderia thailandensis acyl-homoserine lactone-independent orphan LuxR homolog that activates production of the cytotoxin malleilactone. *Journal of Bacteriology*, *197*(21), 3456–3462. https://doi.org/10.1128/JB.00425-15

Wells, J. S., Trejo, W. H., Principe, P. A., Bush, K., Georgopapadakou, N., Bonner, D. P., & Sykes, R. B. (1982). SQ 26,180, a novel monobactam. I Taxonomy, fermentation and biological properties. The Journal of Antibiotics, 35(2), 184–188. https://doi.org/10.7164/ANTIBIOTICS.35.184

Wickham, H. (2016). ggplot2: Elegant Graphics for Data Analysis. Springer-Verlag New York.

Wickham, H. (2019). stringr: Simple, Consistent Wrappers for Common String Operations. R package version 1.4.0.

Wickham, H. (2007). Reshaping data with the reshape package. *Journal of Statistical Software*, *21*(12), 1–20. https://doi.org/10.18637/jss.v021.i12

Wickham, H., Averick, M., Bryan, J., Chang, W., McGowan, L., François, R., … Yutani, H. (2019). Welcome to the Tidyverse. *Journal of Open Source Software*, *4*(43), 1686. https://doi.org/10.21105/joss.01686

Wickham, H., François, R., Henry, L., & Müller, K. (2019). dplyr: A Grammar of Data Manipulation. R package version 0.8.3.

Wozniak, C. E., Lin, Z., Schmidt, E. W., Hughes, K. T., & Liou, T. G. (2018). Thailandamide, a fatty acid synthesis antibiotic that is coexpressed with a resistant target gene. *Antimicrobial Agents and Chemotherapy*, *62*(9), e00463-18. https://doi.org/10.1128/AAC.00463-18

Zdobnov, E. M., & Apweiler, R. (2001). InterProScan - An integration platform for the signature-recognition methods in InterPro. *Bioinformatics*, *17*(9), 847–848. https://doi.org/10.1093/bioinformatics/17.9.847

Zhu, H., Sandiford, S. K., & Van Wezel, G. P. (2014). Triggers and cues that activate antibiotic production by actinomycetes. *Journal of Industrial Microbiology and Biotechnology*, *41*(2), 371–386. https://doi.org/10.1007/s10295-013-1309-z